

CHAPTER 1. INTRODUCTION AND LITERATURE REVIEW

1.1 INTRODUCTION

In this thesis, the feedforward active control of harmonic flexural vibration in three types of stiffened structures using as control sources piezoceramic actuators placed between the stiffener flange and the structure surface is investigated. The first structure considered is a beam of rectangular cross-section with a mock stiffener mounted across the larger cross-sectional dimension. The analysis of vibration in the beam is treated as a one-dimensional problem. The second structure considered is a rectangular plate with a stiffener mounted across the width of the plate. The transverse vibration of the plate is treated as a two-dimensional problem. Finally, a ring-stiffened cylindrical structure is analysed. Vibration in each of the radial, axial and tangential directions is considered. The thesis is presented in three main chapters, each considering one type of structure, but the study of the more complicated structures makes use of results from the simpler cases.

The control of flexural vibrations in a simple beam is considered in Chapter 2, where the classical one-dimensional equation of motion for flexural vibration is used to develop a theoretical model for the vibration of a beam with a primary point source, an angle stiffener and a control actuator. The effective control signal is a combination of the effects of the point force at the base of the actuator, and the reaction force and moment at the base of the stiffener.

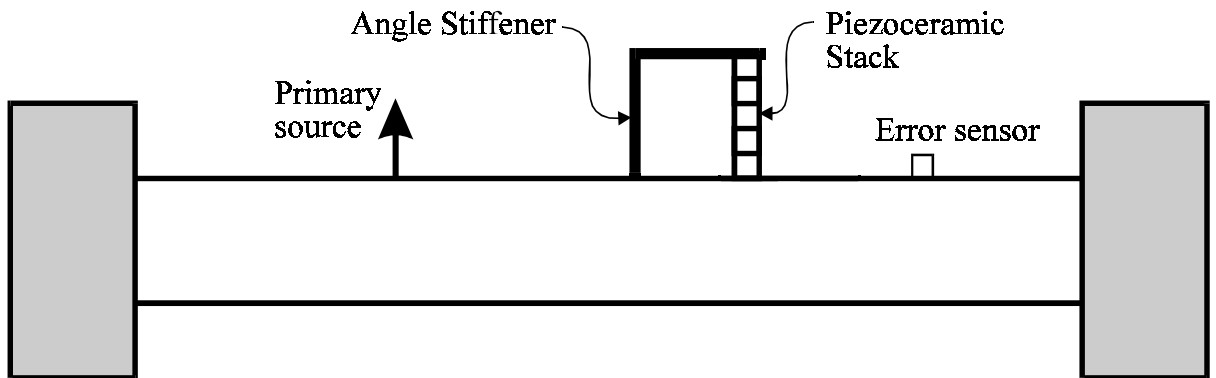


Figure 1.1 Beam showing primary source, angle stiffener, piezoceramic stack control source and error sensor.

The displacement at a point is the sum of the displacements due to each of the primary source and control source forces and moments. Optimal control is achieved by minimising the total mean square displacement at the location of a single error sensor downstream of the control source.

The theoretical analysis considers four different sets of classical beam supports; infinite, free, simply supported and fixed. The influences of the control source location, the error sensor location and the excitation frequency on the control source amplitude and achievable attenuation are investigated, and the physical reasons for each observation are explained. The effects of introducing a second control source and angle stiffener and a second error sensor are also examined.

Experimental verification of the beam model is undertaken for four different sets of beam terminations; infinite, free, simply supported and vibration isolated. The impedance

Chapter 1. Introduction

corresponding to each type of termination is first measured from the experimental apparatus. Experimental results are compared with theoretical predictions for the four cases.

The control of flexural vibrations in a plate is considered in Chapter 3, where the classical two-dimensional equation of motion for flexural vibration is used to develop a theoretical model for the vibration of a plate with one or more primary point sources, an angle stiffener and one or more control actuators. A modal analysis of the plate with and without a stiffener attached shows that the stiffener makes a significant difference to the vibration response of the plate, so the theoretical model is modified to include the effects of the stiffener. The effective control signal is a combination of the effects of the point force at the base of each actuator, and the line force and line moment at the base of the stiffener.

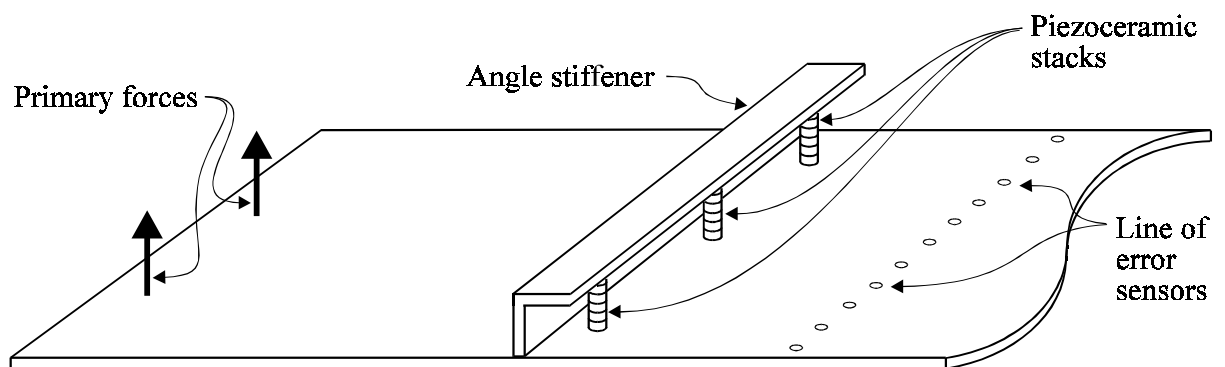


Figure 1.2 Plate showing primary sources, angle stiffener, piezoceramic stack control actuators and error sensors.

Chapter 1. Introduction

The displacement at a point is the sum of the displacements due to each of the primary source and control source forces and moments. Optimal control is achieved by minimising the total mean square displacement at a line of error sensors across the plate downstream of the control sources. Consideration is given to the results achieved with control sources driven by the same signal and with control sources driven independently.

The theoretical analysis considers two different sets of plate supports. In both cases, the edges of the plate are simply supported and the end upstream of the primary sources is modelled as free. In the first case, the end downstream of the error sensors is modelled as infinite, and in the second case the downstream end is modelled as free. The influences of the location of the control sources, the location of the line of error sensors and the excitation frequency on the control source amplitude and achievable attenuation are investigated, and the physical reasons for each observation are explained. The effect of introducing a second angle stiffener and additional control sources is also examined.

Experimental verification of the plate model is performed for the case with the upstream end modelled as free and the downstream end modelled as infinite.

Finally, the more complicated case of control of flexural vibrations in a ring-stiffened cylinder is considered in Chapter 4. The three equations of motion for vibration of a cylinder in the radial, tangential and axial directions are used to develop a theoretical model for the vibration of a cylinder with one or more primary point sources, a ring stiffener and one or

more control actuators. The effective control signal is a combination of the effects of the point force at the base of each actuator, and the line force and line moment around the circumference of the cylinder at the base of the ring stiffener.

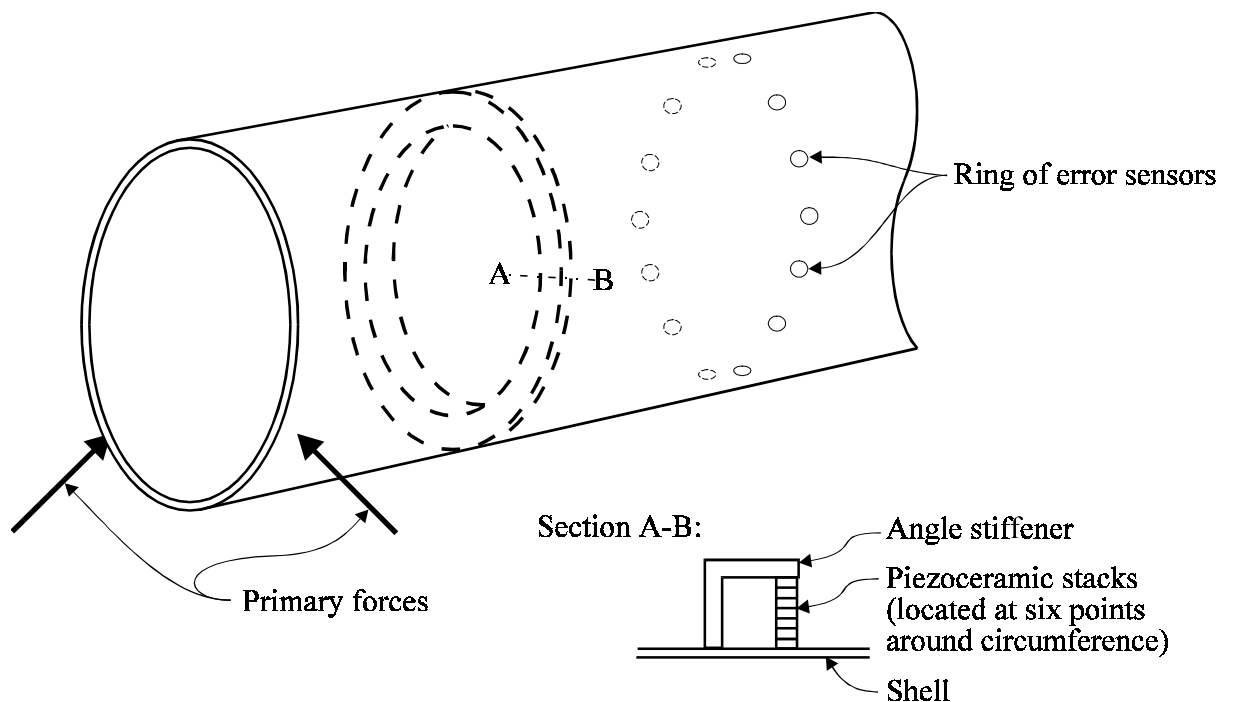


Figure 1.3 Cylinder showing primary sources, ring stiffener, piezoceramic stack control actuators and error sensors.

The displacement at a point is the sum of the displacements due to each of the primary source and control source forces and moments. Optimal control is achieved by minimising the total mean square displacement at a ring of error sensors around the cylinder circumference downstream of the control sources. Consideration is given to the results achieved with control sources driven by the same signal and with control sources driven independently.

Chapter 1. Introduction

The theoretical analysis considers two different sets of cylinder supports. In both cases, the end upstream of the primary sources is modelled as simply supported. In the first case, the end downstream of the error sensors is modelled as infinite, and in the second case the downstream end is modelled as simply supported. The influences of the location of the control sources, the location of the ring of error sensors and the excitation frequency on the control source amplitude and achievable attenuation are investigated, and the physical reasons for each observation are explained.

Experimental verification of the cylinder model is performed for the simply supported cylinder.

In Chapter 5 the results of each structural model are reviewed. The similarities between the three cases are described and the trends established from one model to the next are summarised. The difficulties in controlling vibration in the three types of structure are described, and the implications for controlling vibration in real stiffened structures are presented.

1.2 LITERATURE REVIEW

1.2.1 Analysis of vibration in continuous structures

1.2.1.1 The differential equations of motion

The differential equations of motion for the displacement of simple continuous structures and their basic solutions have been known for a long time. The solutions to the equations of motion for a beam and plate are discussed in various well-known texts (Morse, 1948; Wang, 1953; Timoshenko, 1959; Cremer, Heckl and Ungar, 1973; Graff, 1975, Meirovitch, 1975). Vibration in cylindrical shells is also discussed briefly in the texts by Graff and Cremer, Heckl and Ungar, and in more detail by Timoshenko. Flügge (1960) developed one version of the three-dimensional equations of motion for the vibration of shells and gave solutions for a variety of shell types.

Leissa's famous monographs *Vibration of Plates* (1969) and *Vibration of Shells* (1973a) are comprehensive summaries of the analyses of plate and shell vibration to that time. Leissa's works present results for the free vibration frequencies and modes shapes for plates and shells with a wide array of geometries and boundary conditions.

Noiseux (1970) presented a significant work introducing the concepts of near and far fields of vibrational intensity, using the solutions to the beam and plate equations. The near field exists in the region of a discontinuity, boundary or actuator, and contains reactive and active components. In the far field the reactive component is insignificant. Pavić (1976) determined a method of measuring structural intensity using an array of vibration sensors.

Chapter 1. Introduction

The concepts of near and far fields of vibrational intensity are important in understanding some of the mechanisms involved in active vibration control, particularly when selecting control source and error sensor locations (Sections 2.3, 3.3 and 4.3).

The vibration of beams is a relatively simple problem, and will not be discussed in any great detail in this review. The analysis of vibration in plates and cylinders has received more attention, and is discussed in more detail in Sections 1.2.1.3 and 1.2.1.4 respectively.

1.2.1.2 Treatment of termination impedances in theoretical analysis

The effect on the vibration response of the types of supports used to mount a beam, plate or shell is significant. In any theoretical analysis, the impedances of the structure supports must be modelled. Traditionally, assumptions corresponding to one of a set of classical impedances have been used to model simply supported structures, free structures, fixed structures and semi-infinite structures.

In 1977, Seybert and Ross developed a method for measuring the acoustic impedance of a duct termination, using two microphones placed in a tube with the system under investigation at one end. The method showed that the incident- and reflected-wave spectra and the phase angle between incident and reflected waves, could be determined from measurement of the auto- and cross-spectra of the two microphone signals. Expressions for the normal specific acoustic impedance and reflection coefficient of the impedance material were then developed. Højbjerg (1991) improved the design of the microphones to be used in the impedance tube.

Chapter 1. Introduction

Until recently, there has been no equivalent method for measuring beam impedances. In 1990, Trolle and Luzzato examined the problem, developing a simple method for identifying the four coefficients in the solution for beam displacement from a minimum of four acceleration measurements. They did not apply their work to the measurement of termination impedances. Fuller *et al* (1990) used a similar analysis to find the displacement equation coefficients. With the solution for displacement, they calculated the force and moment impedances of a blocking mass on a beam. They ignored the coupling impedances associated with a termination discussed by Cremer, Heckl and Ungar (1973).

Taylor (1990) presented an alternative method using a measurement of structural intensity to identify the impedance of a beam termination, as well as the related reflection coefficients. While reducing the number of acceleration measurements to three, the method for measuring structural intensity and then calculating impedances is significantly more complicated than the method described by Fuller *et al*. More recent investigations have attempted to improve the accuracy of structural intensity measurements (Halkyard and Mace, 1993; Gibbs and Fuller, 1993; Linjama and Lahti, 1993).

In Section 2.4.1, this thesis examines measurement of the impedance of real beam terminations in order to better compare the experimental and theoretical results for active vibration control. The method used is based on the simple method developed by Fuller *et al* (1990), but here an attempt is made to include the force and moment coupling impedances in the analysis, rather than ignoring them as did Fuller *et al*. The termination impedances of

Chapter 1. Introduction

wire supported, pinned and anechoically terminated beams are measured and compared with the corresponding classical approximations. The number of accelerometers required to give reasonable results using this method is also examined.

When discussing the vibration of plates and cylinders, classical impedance approximations have been used. Development of a method for measuring the impedance of a plate or cylinder support would be far more complicated than that for a beam, and is outside the scope of this work. It is acknowledged that some of the observed differences between theoretical results and experimental data may be due to the inaccuracy of the classical support approximations.

1.2.1.3 Analysis of vibration in rectangular plates

The basics of free vibration in plates are discussed in texts by Timoshenko (1959), Cremer *et al.* (1973), Graff (1975) and others. Early work was concerned exclusively with determining the natural frequencies of plates with a variety of supports and geometries, as can be seen in Leissa's extensive 1969 summary of works to that time. Leissa (1973*b*) also gave a broad analytical study of free vibration in rectangular plates, using the Ritz method to examine the natural frequencies of plates with a variety of classical edge conditions. These analyses utilised the two-dimensional displacement equation with various boundary conditions corresponding to each of the edge constraints. Different forms of the general solution to the displacement equation were used to satisfy the boundary conditions in each case, and the characteristic equation solved for the natural frequencies.

Chapter 1. Introduction

Mukhopadhyay (1978, 1979) developed a new numerical method for determining the natural frequencies of rectangular plates with different degrees of elastic edge restraints, again beginning with the two dimensional displacement equation. The general solution satisfying a given set of boundary conditions was transformed, reduced to an ordinary differential equation, and expressed in finite difference form. The solution of the resulting eigenvalue problem yielded the plate free vibration natural frequencies. Numerical results were presented for some cases, and these results agreed closely with results given in previous work (such as Leissa's).

Other researchers have examined vibration in plates with stiffeners attached using a wide variety of approximate methods. Kirk (1970) used the Ritz method to determine the natural frequencies of a plate with a single stiffener placed on a centre line, and the results compared closely with the exact solution obtained from the plate equation. Wu and Liu (1988) also examined vibration in plates with intermediate stiffening using the Rayleigh-Ritz method. They calculated the first four natural frequencies for some examples, and the results agreed closely with those of Leissa (1973a). Aksu and Ali (1976) used the finite difference method for the free vibration analysis of a rectangular plate with a single stiffener. Cheng and Dade (1990) used bicubic B-splines as coordinate functions to formulate problems based on energy principles, using the technique of piecewise Gauss integration collocation. This method could be used with non-uniform thicknesses of plates. Yet another method, utilising Poynting vector formulation, has been used in structural intensity analysis of plates, by Romano *et al.* (1990).

Chapter 1. Introduction

The most widely used approximate method is the finite element method, applied to plates with discrete stiffeners by Olson and Hazell (1977) and Gupta *et al* (1986). Mead, Zhu and Bardell (1988) examined vibration in a flat plate with an orthogonal array of rectangular stiffeners using this method. Koko and Olson (1992) used super plate and beam finite elements which were constructed so that only a single element per bay or span was required, resulting in an economic model of the orthogonally stiffened structure.

These approximate methods have been developed largely because the exact solution of the plate differential equation is cumbersome, particularly when stiffeners are attached (Koko and Olson, 1992). While these approximate methods were useful in analysing the free vibration of plates with or without attached stiffeners, they have not generally been used to develop models for active vibration control. Some researchers in recent years, particularly those interested in developing a theoretical model for the active feedforward vibration control of plates, have returned to the exact solution of the plate equation; however, none have included stiffeners in their analysis (Section 1.2.2.6).

1.2.1.4 Analysis of vibration in cylindrical shells

There has been much discussion in the literature regarding the equations of motion for cylindrical shells. Unlike the classical equations of motion for the beam and plate, there is no universally accepted set of equations for the cylinder. Because of the complexity of vibrations in cylinders, a large number of assumptions must be made when deriving the equations of motion from the basic strain displacement relationships. Different authors have made distinct assumptions at various points in their derivation, arriving at slightly different equations of motion.

Leissa (1973*a*) gave an extensive summary of the equations derived by the better known authors. He showed that, with a few exceptions, all the theories were very similar and produced results consistent to within a few percent in most cases. In his discussion, Leissa demonstrated that, of all the theories, Flügge's (1934, 1960) work was the most referred to by other researchers, such as Yu (1955), Hoppmann (1957), Forsberg (1964, 1966), Reismann (1968), Reismann and Pawlik (1968), Smith and Haft (1968) and Warburton (1969). Recent researchers have also used the equations of motion developed by Flügge (e.g. Fuller, 1981; Haung, 1991; Païdoussis *et al*, 1992).

The main criticism of Flügge's version of the equations of motion for a cylinder has been his omission of inertia terms. Leissa (1973*a*) showed that the omission of these terms can cause inaccurate results, and most researchers include the inertia terms in their analyses.

Chapter 1. Introduction

The early work described using the Flügge equations has been directed towards calculation of the natural frequencies of a variety of cylinders. More recent authors include complicating effects in their analyses, such as the effect of wall discontinuities on the propagation of waves (Fuller, 1981) and the coupled vibrations of shells containing liquids (Haung, 1991 and Paidoussis *et al*, 1992). No author has previously developed and presented quantitative solutions for the acceleration (or velocity or displacement) amplitude distribution over a cylinder in response to a specific form of vibration excitation, from the Flügge equations or any other of the similar equations of motion for cylinders. In Section 4.2 of this thesis, the Flügge equations, with the inertia terms included, are used to develop a model for the vibration of a cylinder in response to the application of a point force, a line force and a line moment.

Wah and Hu (1968) examined the free vibration of ring-stiffened cylinders using a highly simplified set of the equations of motion for shells. They divided the ring-stiffened cylinder into bays and considered the effect of the stiffener on the boundary conditions at the junction of two bays. In this thesis the effects of ring-stiffeners on the vibration response of a cylinder are included in the solution to the full set of Flügge equations, without dividing the cylinder into bays (Section 4.2).

A variety of approximate methods have also been used in the analysis of vibration of stiffened shells. Galletly (1954), Mikulas and M^cElman (1965) and Patel and Neubert (1970) used energy methods in their determinations of the natural frequencies of stiffened shells. More

Chapter 1. Introduction

recently, Mead and Bardell (1986, 1987) presented a computational method of determining the natural frequencies of shells from propagation constants. Cheng and Jian-Guo (1987) applied B spline functions to flat shells, and Cheng and Dade (1990) extended this method to include stiffened shells and plates. Romano *et al* (1990) applied their Poynting vector method to the analysis of structural intensity in shells as well as plates.

Finite element analysis has also been used in the analysis of shell vibration (e.g. Bogner *et al*, 1967; Cantin and Clough, 1968; Henschell, Neale and Warburton, 1971 and Orris and Petyt, 1974). Recently, Mustafa and Ali (1987) applied structural symmetry techniques to the prediction of the natural frequencies of stiffened and unstiffened shells and developed boundary conditions for the analysis of part-shells. Mecitoglu and Dökmeci (1991) used a finite element analysis including smeared stringers and frames. Langley (1992) took stiffeners to be smeared over the surface of an element, with a view to analysing complex aircraft structures using only a few elements. Sinha and Mukhopadhyay (1994) used high precision curved triangular elements in their analysis, allowing greater flexibility in placement of stiffeners in the shell model.

As was the case with the analysis of vibrations in plates, the approximate methods used for the investigation of vibration in cylinders have been developed because the exact solution of the differential equations of motion is unwieldy. While these approximate methods have been useful in analysing the free vibration of cylindrical shells, they have not been used to develop models for active vibration control.

Chapter 1. Introduction

1.2.2 Active vibration control

1.2.2.1 The origins of active noise and vibration control

The fields of active noise control and active vibration control have much in common. Active noise control can be traced back to Lueg's work in the nineteen thirties, although his ideas were far in advance of the technology required for practical noise control systems (Guicking, 1990). Nearly twenty years later, Olson (1953, 1956) experimented with an "electronic sound absorber". His arrangement consisted of a microphone mounted in close proximity to the face of a loudspeaker cone. The loudspeaker was driven to null the sound pressure at the microphone, creating a quiet area around it. His results were promising, but the electronics technology of his time was still not sufficiently advanced to enable implementation in useful applications. Conover's 1956 application of loudspeakers arranged around a noisy transformer was another early attempt at noise control. However, it was not until the late nineteen sixties and early seventies that electronics technology became advanced enough to make implementation of basic noise control systems practical (Snyder, 1990).

Despite this early investigation into the active control of noise, and discussion of active control of structural damping in the late seventies (Section 1.2.2.2), it wasn't until the eighties that advances in vibration actuator technology made active vibration control a feasible alternative in practical situations. The introduction of the piezoelectric actuator to vibration control by Bailey and Hubbard (1985) marked a new era in active vibration control (Section 1.2.2.3).

1.2.2.2 Development of feedback vibration control methods

Most early active vibration control theory considered modal feedback control of large structures. Balas and Canavin (1977) discussed feedback damping control of large spacecraft structures. Balas (1978) applied theoretical modal control using velocity feedback to a simple beam. Meirovitch and Öz (1980), with later work by Meirovitch and others (Meirovitch, Baruh and Öz, 1983; Meirovitch and Norris, 1984; Zhu and Bardell, 1985; Meirovitch and Bennighof, 1986), expanded the modal control method, with Meirovitch and Bennighof arriving at a method they described as Independent Modal-Space Control (IMSC), where a coordinate transformation was used to decouple a complicated system into a set of independent second order systems in terms of modal coordinates. Baz and Poh (1988) made modifications to the IMSC method to minimise the effect of control spillover into unmodelled modes and also into modelled modes when the number of modelled modes exceeded the number of control sources used.

In 1986 von Flotow presented another feedback control solution which considered modification of the disturbance propagation characteristics of the structure. The discussion indicated that the amount of control achieved using this method would be limited at low frequencies. The results were later compared with the velocity feedback method and with experiments on a beam (von Flotow and Schäfer, 1986).

Feedback control methods like those discussed are suited to the control of vibrations in very large structures with many structural members and in situations where it is difficult to obtain

Chapter 1. Introduction

a suitable reference signal. In feedback systems, design of the control system is dependent to a large degree on the physical analysis of the structure. In the design of feedforward control systems, the physical analysis of the structure can be separated from the design of the electronic controller. In recent years, a significant amount of research effort has been concerned with feedforward control. In this thesis, the emphasis is on analysis of the physical mechanisms behind the feedforward active control of harmonic vibration in structures consisting of relatively few fundamental elements, in structures where reference signals can be obtained. However, the results relating to the performance of the piezoceramic stack control actuators are still relevant to feedback control systems.

1.2.2.3 Actuators for active vibration control

Electromagnetic shakers were used as control actuators in much of the early experimental work on active vibration control (Noiseux, 1970). While electromagnetic shakers are useful tools in experimental work, their usefulness in practical applications is severely limited by their size and mass.

Bailey and Hubbard (1985) introduced piezoelectric actuators to active vibration control. They used the actuators bonded to the surface of a cantilever beam in their feedback vibration damping design. Crawley and de Luis (1987) presented an analytical and experimental development of piezoelectric actuators as vibration exciters. Using the models they developed from stress/strain relationships, Crawley and de Luis were able to predict the displacement of three real cantilevered beam and piezoelectric actuator arrangements under

Chapter 1. Introduction

steady-state resonance vibration conditions. Their work demonstrated several important results regarding the stress/strain behaviour of piezoelectric actuators, including the effect of stiffer and thinner bonding layers.

Dimitriadis *et al* (1991) and performed a two-dimensional extension of Crawley and de Luis' work, applying pairs of laminated piezoelectric actuators to a plate. They demonstrated that the location and shape of the actuator dramatically affected the vibration response of the plate. Kim and Jones (1991) performed another study into the use of laminated piezoelectric actuators, following a similar analytical method to that used by Crawley and de Luis (1987) and Dimitriadis *et al* (1991). They calculated the optimal thickness of piezoelectric actuators, and investigated the influence of the thickness and material properties of the bonding layer and piezoelectric actuators on the effective moment generated and the optimal actuator thickness.

Clark *et al* (1991) performed tests on a simply supported beam excited by pairs of piezoelectric actuators bonded to either side. They compared test results with theoretical predictions made using the one-dimensional beam equation altered to include the effects of the piezoelectric crystals. They discussed the idea of modelling a piezoelectric element by two pairs of line moments acting along the edges of the element. Their test results agreed to within 25% of the theoretical predictions. The paper concluded that discrepancies between experiment and theory were the result of some of the assumptions they made in modelling the piezoelectric elements and the beam using the one-dimensional beam theory. The

Chapter 1. Introduction

assumptions ignored the increase in beam stiffness due to strain in the normal direction to the vibration and the fact that the piezoelectric elements were not as wide as the beam. The authors suggested that a finite element analysis may be required to predict the beam response more accurately, but for the purposes of choosing optimal actuator locations and relative structural responses, the one-dimensional model was sufficient.

Lester and Lefebvre (1993) extended to a cylinder the theoretical models of Dimitriadis *et al* (1991) applying piezoelectric actuators to plates. They developed two models; in the first the actuator acted on the cylinder through line moments along the actuator edges, and in the second through in-plane forces along the actuator edges. They used a modal amplitude analysis to show that the in-plane force model predicted better coupling between the actuator and lower order modes than the bending model, and suggested that the in-plane force model may be more suitable in the development of a model for the use of distributed piezoelectric actuators as vibration control actuators. Rivory *et al* (1994) reviewed and extended previous models of beam - laminated actuator systems and compared theoretical results with experimental data to show that the models did not predict accurately the response of the beam to excitation by laminated actuators at frequencies away from the beam resonances.

The purpose of this thesis is to investigate the use of a piezoceramic stack actuator placed between the flange of a stiffener and the surface of a structure to control vibration in the structure. In this thesis, it is the one-dimensional model that is used to describe the response of the beam to the piezoceramic stack actuators (Section 2.2.3). Since these actuators act

Chapter 1. Introduction

essentially at a point, not over an area like laminated piezoelectric actuators, some of the problems experienced by Clark *et al*, Rivory *et al* and others will not be important.

Many other researchers have used piezoelectric actuators in active vibration control experiments. Fansen and Chen (1986) and Baz and Poh (1988, 1990) presented results for active control of beams using piezoelectric actuators, showing again the potential of piezoelectric actuators as control actuators in vibration control where low forces are required. Tzou and Gadre (1989) developed a theoretical model for the active feedback control of a multi-layered shell with distributed piezoelectric control actuators using Love's theory. Their analysis included a detailed examination of the stresses and strains between layers. Other investigators to examine the use of laminated piezoelectric actuators in vibration excitation and control include Wang *et al* (1991), Liao and Sung (1991), Pan *et al* (1992), Tzou and Fu (1994*a* and 1994*b*) and Clark and Fuller (1994). Clearly there is a perceived need for a vibration actuator that can be used in practical situations, where the large reaction mass of an electromagnetic shaker is unsuitable (Rivory, 1992). The laminated piezoelectric actuator has become the popular alternative, but this type of actuator is fragile and is not capable of generating great amounts of force. This thesis examines the suitability of another type of actuator, the piezoceramic stack actuator, which is capable of producing much higher forces for vibration excitation or vibration control than the thin laminated actuators.

The application of piezoceramic stack actuators to control of vibrations in rotating machinery was considered in a paper by Palazzolo *et al* in 1989. Their experimental results indicated

Chapter 1. Introduction

that significant reductions in the vibration of rotating machinery could be achieved using two of these actuators in the support structure of the rotating shaft. To the author's knowledge, no research has been performed considering the use of the stack actuator to control vibrations in any other type of structure, such as the structures considered in this thesis.

1.2.2.4 Error sensors for active vibration control

Traditionally, accelerometers have been used for vibration measurement and as error sensors for active control of vibration. Along with the introduction of piezoelectric materials for vibration excitation, the use of piezoelectrics such as polyvinylidene fluoride (PVDF) for vibration sensing has developed (Bailey and Hubbard, 1985; Burke and Hubbard, 1988; Clark and Fuller, 1992). Cox and Lindner (1991) discussed optical fibre sensors for vibration control. Distributed vibration sensors such as the piezoelectric and optical fibre sensors can be shaped and placed to generate suitable error signals when only certain modes of vibration are to be controlled; for example, when reducing the far field noise emitted from a plate (Clark and Fuller, 1992).

Thomas *et al* used minimisation of vibrational kinetic energy (1993a) and acoustic potential energy (1993b) as the cost functions for the feedforward active control of harmonic vibration. Clark and Fuller (1994) presented the results of experimental work dealing with the control of harmonic vibrations in an enclosed cylinder using between three and six piezoelectric patches as control sources and microphones or polyvinylidene fluoride vibration sensors as cost

Chapter 1. Introduction

functions. Both investigations showed that simple vibration error sensors generally give poor results for the attenuation of transmitted or radiated sound in comparison to acoustic sensors, because use of vibration sensors does not necessarily lead to minimisation of the modes that contribute most to the radiated or transmitted sound power.

The aim in this thesis is to minimise the total vibratory power transmission downstream of the control sources. Pan and Hansen (1993a,1995a) demonstrated that simple acceleration measurements can be used to optimally reduce total vibration transmission provided the error sensors are not located in the vibratory near field produced by the control sources. Accelerometer measurements are used here as the cost functions for active vibration control.

1.2.2.5 Feedforward active control of vibration in beams

Much of the research in recent years has focussed on feedforward control of harmonic flexural vibration in simple structures.

Redman-White *et al* (1987) used feedforward control in their experimental work. They used two closely-spaced point force control actuators to control harmonic flexural vibration in a beam excited by a single point source primary excitation. They showed that minimising vibration at the location of the control source is not sufficient for reducing power transmission downstream; rather, velocity should be minimised at a point far downstream of the control sources. Xia Pan and Hansen (1993*a*) showed that minimisation of velocity at a point and minimisation of flexural wave power give identical results provided the error sensor is located in the far field of the primary and control sources. Minimisation of power transmission gives better results when the error sensor is in the near field of the control source. In this thesis work, minimisation of velocity (acceleration) at a point is used, with the error sensor generally in the far field of the primary and control sources.

Mace (1987) examined theoretically the active control of harmonic flexural vibration in beams. He discussed the excitation and control of vibration from two types of actuator; point force and point moment. Mace treated the point force and point moment as discontinuities in the shear force and bending moment in the beam with resulting discontinuities in the displacement solution for the beam equation at the point of application of the force or moment. This analysis is followed in this thesis for the treatment of vibration in beams

Chapter 1. Introduction

(Section 2.2.3) and extended to include line moments and line forces on plates and cylinders (Sections 3.2.3 and 4.2.4).

Gonidou (1988) used a similar analysis in his treatment of beam vibration control. He concluded that good feedforward control can be achieved with a single control source if power transmission is used as the cost function. As already mentioned, Xia Pan and Hansen (1993*a*) showed that minimising velocity was equivalent to minimising power transmission provided the error sensor was located outside of the control source near field. In the current work, a single control source is considered and acceleration at a point is used as the cost function. The dependence of attenuation on control source - error sensor separation is examined in Section 2.3.3.

In 1990 Gibbs and Fuller controlled harmonic flexural vibration in experiments on a thin beam using laminated piezoelectric actuators and an adaptive feedforward least squares controller, achieving 30 dB or more attenuation for beams with a variety of termination types. Jie Pan and Hansen (1990*a*) performed some similar experiments on beams, but used a single point force as the control source. Both papers demonstrated that reducing harmonic power transmission using a secondary source had the effect of reducing the power input from the primary source. This idea is consistent with the analogous case for ducts (Snyder, 1990) and is widely accepted.

Xia Pan and Hansen (1993*b*) solved the one-dimensional beam displacement equation,

Chapter 1. Introduction

treating the point of application of the primary and control point sources as discontinuities in the beam displacement in a similar manner to Mace (1987). Their analysis discussed some of the effects of variations in control source location, error sensor location, beam termination type and frequency on the attenuation of vibration level, but without attempting to explain the physical reasons for the observations. In Section 2.3 this thesis examines the effect of control source location, error sensor location, frequency and type of termination on the magnitude of the control signal and the achievable attenuation, offering explanations for all observations. The aim is to develop a full understanding of the physical behaviour of a beam vibration control system. This work will aid in understanding the behaviour of the more complicated stiffened plate and stiffened cylinder vibration control systems in later chapters.

Recent work by Petersson (1993*a*) discussed the significance of the moment in a combined moment and force excitation of a beam. Numerical results indicate that moments must be taken into account at all frequencies. When a piezoceramic actuator is placed between the flange of a stiffener and the beam surface, there is a moment reaction as well as a force reaction at the base of the stiffener. Petersson's work indicates that the moment may be a significant part of the effective control signal. In Section 2.2.3.2 of this thesis, the one-dimensional displacement equation is solved for a point moment excitation, treating the moment as a discontinuity in the beam displacement, following the analysis of Xia Pan and Hansen (1993*b*) for a point force, and Mace (1987). In Section 2.2.5, the effective control signal is analysed in terms of the point forces and the point moment developed by the piezoceramic actuator and angle stiffener combination.

Chapter 1. Introduction

Fuller *et al* (1990), Jie Pan and Hansen (1990a) and Xia Pan and Hansen (1993a) have made limited comparisons between theoretical results and experimental data for active feedforward control of vibration in beams. In Section 2.5 of this thesis, direct comparison is made between the numerical results and experimental data for vibration of beams both with and without active vibration control for an aluminium beam with four types of termination.

1.2.2.6 Feedforward active control of vibration in plates

Dimitriadis *et al* (1991) used the two dimensional plate displacement equation in their study of the application of piezoelectric actuators in control of harmonic flexural vibration in unstiffened plates. The displacement equation was solved for the vibration responses to line moments parallel to the x - and y -axes. The results of their work showed that control of vibrations in plates using bonded piezoelectric actuators was possible, and that the location of the actuators and the excitation frequency are important factors in the effectiveness of the control achieved. They did not investigate in any depth the dependency of control effectiveness on actuator location and frequency.

In a two-part presentation, Fuller (1990) and Metcalf *et al* (1992) investigated analytically and experimentally the effectiveness of active feedforward control of sound transmission and radiation from a plate using one and two point force control sources and acoustic error sensors. Metcalf *et al* showed that use of acoustic sensors gives greater attenuation of radiated sound than vibration sensors. The purpose of this thesis is to investigate control of vibration, not control of radiated sound, and accordingly vibration sensors are used rather

Chapter 1. Introduction

than acoustic sensors.

Recent work by Pan and Hansen (1994) used a classical plate equation solution to compare piezoelectric crystal with point force excitation of beams and plates. An "equivalence ratio" was derived, which could be used to determine the magnitude of a point force which would give the same root mean square displacement amplitude as a piezoelectric actuator at some position downstream of the actuator. Pan and Hansen (1995a) used a similar analysis to investigate active control of power transmission along a semi-infinite plate with a variety of piezoelectric actuator configurations. It was found that the effectiveness of the vibration control depended greatly on location of the control actuator and excitation frequency. In this thesis, the dependence of attenuation and control source amplitude and phase on frequency, control source location and error sensor location are investigated for the control of vibration in plates using three piezoceramic stack control actuators and an angle stiffener (Section 3.3).

In analysing the effectiveness of piezoceramic stack control of a stiffened plate, the plate displacement equation is solved directly to develop models for the plate excited by point forces and line moments parallel to the y -axis, following the work of Dimitriadis *et al* (1991) and Pan and Hansen (1994). In addition, a new solution is developed for the application of line forces parallel to the y -axis (Section 3.2). The effect of attached stiffeners on the vibration response of the plate is included in the classical model for the first time.

Fuller *et al* (1989) were the first to demonstrate the potential effectiveness of piezoelectric

actuator control of sound radiated from plates in experimental work. Their results show global reductions in sound radiated from a panel of the order of 30 dB. To this author's knowledge, there have been few experimental works dealing with feedforward active control of vibration in plates and none directly comparing experimental data with theoretical predictions for the acceleration distribution over a plate with vibration control. In Section 3.5 of this thesis, direct comparison is made between theoretical predictions and experimental data for the vibration response of a stiffened plate with and without active vibration control.

1.2.2.7 Feedforward active control of vibration in cylinders

The feedforward active control of vibration in cylinders and aircraft fuselages has gained increasing attention in recent years, but largely in the interests of reducing the sound radiated from a vibrating shell or transmitted through it rather than reducing the vibration transmitted along the cylinder.

Fuller and Jones (1987) performed an experimental investigation into the control of acoustic pressure inside a closed cylinder using an external acoustic monopole primary source, a single point force vibration control source and microphone sensors mounted on a traverse inside the cylinder. This work was extended later to include more control sources (Jones and Fuller; 1989). Significant global attenuation was achieved for harmonic excitation. Elliott *et al* (1989) have performed successful experiments on the control of aircraft noise in-flight, but using acoustic rather than vibration control sources. Thomas *et al* (1993a,1993b) and Clark and Fuller (1994) investigated the effect of using different acoustic and vibration error

Chapter 1. Introduction

sensors in the active vibration control of cylinders (discussed briefly in Section 1.2.2.4).

The work done by researchers such as Fuller with Jones and Clark, and Thomas *et al* shows that active vibration control of aircraft noise is an application of vibration control that has great potential for implementation in real systems in the near future. The purpose of this thesis is to investigate the feasibility of using piezoceramic stack actuators as control sources in real active vibration control situations to reduce vibration transmission along large cylinders such as those found in large aircraft and submarines. The aim of this work can be met by demonstrating that piezoceramic stack actuators can be used as control sources to significantly reduce vibration in cylinders (Chapter 4). Investigation of the effects of excitation frequency, number of control sources, control source location and error sensor location on the amount of control achieved is included (Section 4.3) to establish trends that may be significant when taking the next step to practical implementation.

There has been little work done on the feedforward active control of vibrations in cylinders. To the author's knowledge, none has directly compared theoretical results with experimental data. In this thesis, the theoretical model developed to examine the use of the stack actuators in cylinder vibration control is verified experimentally (Section 4.5).

1.3 SUMMARY OF THE MAIN GAPS IN CURRENT KNOWLEDGE ADDRESSED BY THIS THESIS

The primary aim of this thesis is to investigate the potential of the piezoceramic stack actuator in feedforward active control of harmonic vibration. The actuator is suitable specifically for use in stiffened structures (or structures with stiffeners added). This application of piezoceramic stack actuators is new. A theoretical model is developed to describe the response of beams, plates and cylinders to excitation by the stack actuator. The solutions of the classical equations of motion for plate and cylinder structures including the effects of stiffening, and the analysis of the forces and moments applied to all three structure types by the stack actuator and angle stiffener control source are new. The solution of the three dimensional equations of motion for a cylinder to determine the vibration response to force and moment excitations is original.

For each type of structure, the physical reasons for the given results are discussed, particularly in relation to the variation of control effort and attenuation as functions of control location, error sensor location and frequency. Some of this discussion represents an extension of previous work and much of it is new.

Prior to this work, there has been some work published directly comparing theoretical results and experimental data for active vibration control of beams, but almost none for the active vibration control of plates or cylinders. Here direct comparison is made between the theoretical models and experimental data for vibration in beams, plates and cylinders, for a variety of cases with and without active vibration control.

CHAPTER 2. FEEDFORWARD ACTIVE CONTROL OF FLEXURAL VIBRATION IN A BEAM USING A PIEZOCERAMIC ACTUATOR AND AN ANGLE STIFFENER

2.1 INTRODUCTION

In this chapter, the active control of flexural vibration in beams using as a control source a piezoceramic actuator placed between a stiffener flange and the beam surface is investigated. The beam is of rectangular cross-section with a mock stiffener mounted across the larger cross-sectional dimension. The analysis of vibration in the beam is treated as a one-dimensional problem. The classical one-dimensional equation of motion for the flexural vibration of a beam is used to develop a theoretical model for the beam with a primary point source and an angle stiffener and control actuator (Section 2.2). The effective control signal is a combination of the effects of the point force at the base of the actuator, and the reaction force and moment at the base of the stiffener (Section 2.2.5).

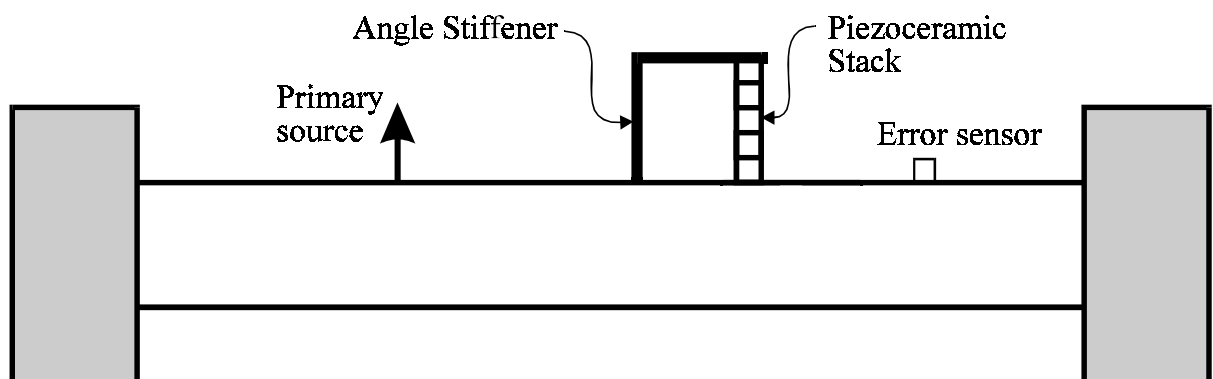


Figure 2.1 Beam showing primary source, angle stiffener, piezoceramic stack control source and error sensor.

Chapter 2. Control of vibrations in a stiffened beam

The displacement at a point is the sum of the displacements due to each of the primary source and control source forces and moments. Optimal control is achieved by minimising the total mean square displacement at the location of a single error sensor downstream of the control source.

The theoretical analysis considers four different sets of classical beam supports; infinite, free, simply supported and fixed. The influence of the control source location, the error sensor location and the excitation frequency on the control source amplitude and achievable attenuation are investigated, and the physical reasons for each observation are explained (Section 2.3). The effect of introducing a second control source and angle stiffener is also examined (Section 2.3.4).

Experimental verification of the beam model is performed for four different sets of beam terminations; infinite, free, simply supported and vibration isolated (Section 2.4). The impedance corresponding to each type of termination is first measured from the experimental apparatus (Section 2.4.1). Finally, experimental results are compared with theoretical predictions (Section 2.5).

2.2 THEORY

2.2.1 Response of a beam to a harmonic excitation

In this section the response of an arbitrarily terminated beam to a simple harmonic excitation $q(x)e^{j\omega t}$ applied at $x = x_0$ as shown in Figure 2.2 is considered. Left and right boundary conditions are specified as impedance matrices Z_L and Z_R .

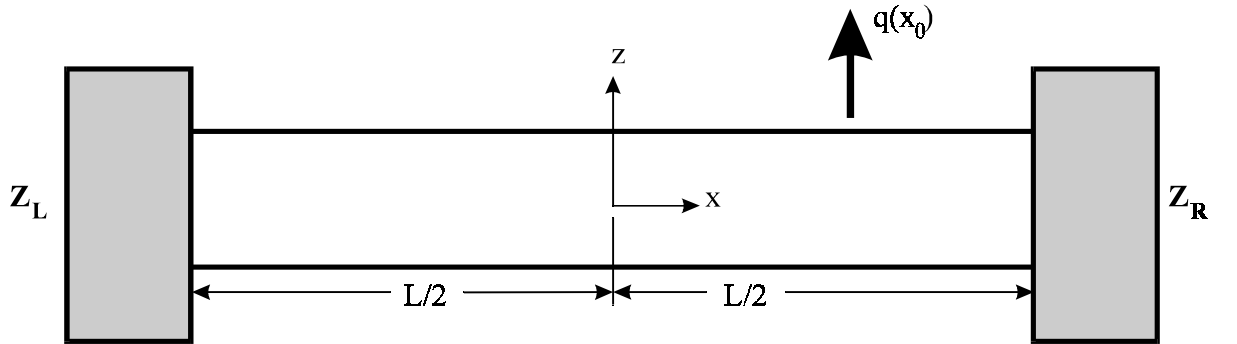


Figure 2.2 Beam with an excitation q at location x_0 .

Following the sign conventions shown in Figure 2.3, the equation of motion for the flexural vibration of the beam shown in Figure 2.2 is

$$EI_{yy} \frac{\partial^4 w}{\partial x^4} + \rho S \frac{\partial^2 w}{\partial t^2} = q(x) e^{j\omega t} , \quad (2.1)$$

where E is Young's modulus of elasticity, I_{yy} is the second moment of area of the beam cross-section, S is the cross-sectional area, ρ is the density and w is the displacement of the beam in the z -direction. The general solution to Equation (2.1) is of the form

$$w(x) = Ae^{k_b x} + Be^{-k_b x} + Ce^{jk_b x} + De^{-jk_b x} . \quad (2.2)$$

Chapter 2. Control of vibrations in a stiffened beam

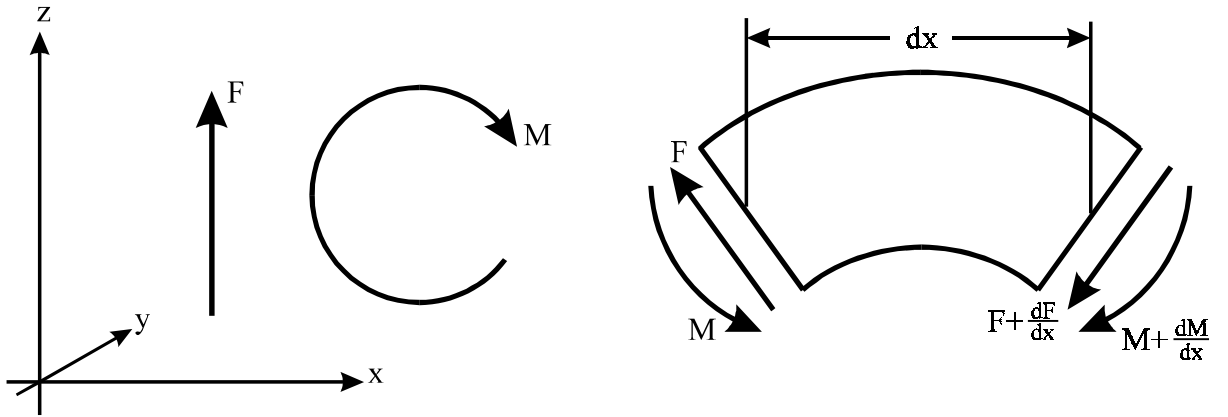


Figure 2.3 Sign conventions for forces and moments.

On each side of the applied excitation at $x = x_0$, a separate solution of Equation (2.1) is required. For $x < x_0$ (on the left hand side of the applied excitation),

$$w_1(x) = A_1 e^{k_b x} + B_1 e^{-k_b x} + C_1 e^{jk_b x} + D_1 e^{-jk_b x} , \quad (2.3)$$

and for $x > x_0$ (on the right hand side of the applied excitation), the solution is

$$w_2(x) = A_2 e^{k_b x} + B_2 e^{-k_b x} + C_2 e^{jk_b x} + D_2 e^{-jk_b x} . \quad (2.4)$$

To find the flexural wave number k_b , the homogeneous form of Equation (2.1) is solved to give the characteristic equation

$$EI_{yy} k_b^4 - \rho S \omega^2 = 0 , \quad (2.5)$$

so

$$k_b = \left(\frac{\rho S \omega^2}{EI_{yy}} \right)^{\frac{1}{4}} . \quad (2.6)$$

Chapter 2. Control of vibrations in a stiffened beam

To solve for the eight unknowns $A_1, B_1, C_1, D_1, A_2, B_2, C_2, D_2$, eight equations are required, comprising of four boundary condition equations (force and moment conditions at each end of the beam) and four equilibrium equations at the point of application x_0 of the force or moment.

2.2.2 Boundary conditions at the beam ends

2.2.2.1 Beam boundary impedance

A boundary impedance for a beam may be defined in terms of force and moment impedances because the boundary acts like an external force and moment generator, effectively applying external forces and moments to the beam which are equal to the internal shear force F and moment M at the ends of the beam. If a moment and force act simultaneously on any part of a beam, coupling will exist between the moment and force impedances. This is because the moment will result in a lateral displacement as well as a rotation and the lateral force will result in a rotation as well as a lateral displacement. Thus, the local lateral velocity and angular velocity generated at the end of a beam as a result of the end conditions may be written respectively as (Cremer *et. al.*, 1973)

$$\dot{w} = \frac{M}{Z_{mf}} + \frac{F}{Z_f} \quad (2.7)$$

and

$$\dot{\theta} = \frac{M}{Z_m} + \frac{F}{Z_{fm}}, \quad (2.8)$$

Chapter 2. Control of vibrations in a stiffened beam

where Z_{mf} and Z_{fm} are the coupling impedances and Z_f and Z_m are the force and moment impedances respectively. For harmonic signals $\dot{w} = j\omega w$ and $\dot{\theta} = -j\omega w'$, where the prime indicates differentiation with respect to the x -coordinate. Rearranging Equations (2.7) and (2.8) gives

$$\begin{bmatrix} F \\ M \end{bmatrix} = \begin{bmatrix} Z_{f\dot{w}} & Z_{f\dot{\theta}} \\ Z_{m\dot{w}} & Z_{m\dot{\theta}} \end{bmatrix} \begin{bmatrix} \dot{w} \\ \dot{\theta} \end{bmatrix}, \quad (2.9)$$

or

$$\begin{bmatrix} F \\ M \end{bmatrix} = \mathbf{Z} \begin{bmatrix} \dot{w} \\ \dot{\theta} \end{bmatrix}, \quad (2.10)$$

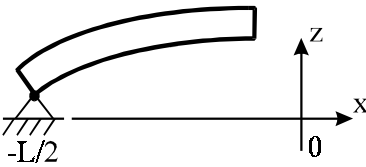
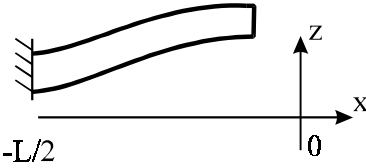
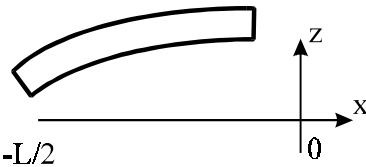
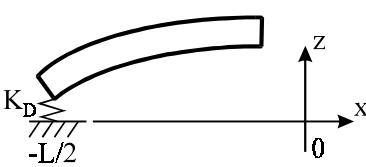
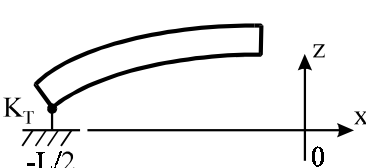
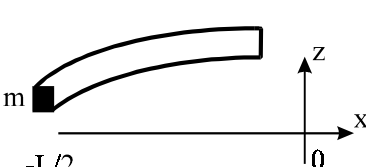
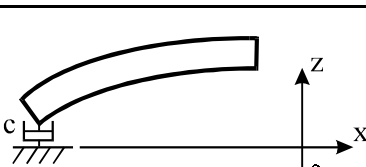
where

$$\mathbf{Z} = \begin{bmatrix} Z_{f\dot{w}} & Z_{f\dot{\theta}} \\ Z_{m\dot{w}} & Z_{m\dot{\theta}} \end{bmatrix} = \begin{bmatrix} \frac{1}{Z_m} & \frac{1}{Z_{fm}} \\ \frac{1}{Z_{mf}} & \frac{1}{Z_f} \end{bmatrix}^{-1}. \quad (2.11)$$

The matrix \mathbf{Z} describes the dependence of the shear force and moment at the boundary on the motion of a beam in simple flexure. The relationships between standard support types and corresponding boundary impedances are given in Table 2.1, with cross terms $Z_{m\dot{w}}$ and $Z_{f\dot{\theta}}$ zero for the standard support types shown.

Table 2.1

Impedances Corresponding to Standard Terminations

End Condition	Representation	Boundary Condition	Impedance
Simply Supported		$w = 0$ $\frac{\partial^2 w}{\partial x^2} = 0$	$Z_{f\dot{w}} = \infty$ $Z_{m\dot{\theta}} = 0$
Fixed		$w = 0$ $\frac{\partial w}{\partial x} = 0$	$Z_{f\dot{w}} = \infty$ $Z_{m\dot{\theta}} = \infty$
Free		$\frac{\partial^2 w}{\partial x^2} = 0$ $\frac{\partial w^3}{\partial x^3} = 0$	$Z_{f\dot{w}} = 0$ $Z_{m\dot{\theta}} = 0$
Deflected Spring		$\frac{\partial^2 w}{\partial x^2} = 0$ $EI_{yy} \frac{\partial^3 w}{\partial x^3} = -K_D w$	$Z_{f\dot{w}} = j \frac{K_D}{\omega}$ $Z_{m\dot{\theta}} = 0$
Torsion Spring		$w = 0$ $EI_{yy} \frac{\partial^2 w}{\partial x^2} = K_T \frac{\partial w}{\partial x}$	$Z_{f\dot{w}} = \infty$ $Z_{m\dot{\theta}} = -j \frac{K_T}{\omega}$
Mass		$\frac{\partial^2 w}{\partial x^2} = 0$ $EI_{yy} \frac{\partial^3 w}{\partial x^3} = -m \frac{\partial^2 w}{\partial t^2}$	$Z_{f\dot{w}} = -j\omega m$ $Z_{m\dot{\theta}} = 0$
Dashpot		$\frac{\partial^2 w}{\partial x^2} = 0$ $EI_{yy} \frac{\partial^3 w}{\partial x^3} = -c \frac{\partial w}{\partial t}$	$Z_{f\dot{w}} = -c$ $Z_{m\dot{\theta}} = 0$

2.2.2.2 Equivalent boundary impedance of an infinite beam

The displacement amplitude function for a right travelling wave in an infinite beam can be written as

$$w(x) = Be^{-k_b x} + De^{-jk_b x} \quad (2.12)$$

so that

$$\dot{w}(x) = j\omega Be^{-k_b x} + j\omega De^{-jk_b x} \quad (2.13)$$

and

$$\dot{\theta}(x) = j\omega k_b Be^{-k_b x} - \omega k_b De^{-jk_b x}, \quad (2.14)$$

where k_b is the flexural wave number of the beam and B and D are constants. Equations (2.13) and (2.14) can be written in matrix form as

$$\begin{bmatrix} \dot{w}(x) \\ \dot{\theta}(x) \end{bmatrix} = \begin{bmatrix} j\omega & j\omega \\ j\omega k_b & -\omega k_b \end{bmatrix} \begin{bmatrix} Be^{-k_b x} \\ De^{-jk_b x} \end{bmatrix}. \quad (2.15)$$

Inversion gives

$$\begin{bmatrix} Be^{-k_b x} \\ De^{-jk_b x} \end{bmatrix} = \begin{bmatrix} -\frac{(1+j)}{2\omega} & \frac{(1-j)}{2\omega k_b} \\ \frac{(1-j)}{2\omega} & -\frac{(1-j)}{2\omega k_b} \end{bmatrix} \begin{bmatrix} \dot{w}(x) \\ \dot{\theta}(x) \end{bmatrix}. \quad (2.16)$$

Differentiating Equation (2.12) to eliminate w'' and w''' from $M = -EI_{yy} w''$ and

$F = EI_{yy} w'''$ respectively, the following matrix equation can be established;

Chapter 2. Control of vibrations in a stiffened beam

$$\begin{bmatrix} F(x) \\ M(x) \end{bmatrix} = -EI_{yy} \begin{bmatrix} k_b^3 & -jk_b^3 \\ k_b^2 & -k_b^2 \end{bmatrix} \begin{bmatrix} Be^{-k_b x} \\ De^{-jk_b x} \end{bmatrix}. \quad (2.17)$$

Combining with Equation (2.16) gives

$$\begin{bmatrix} F(x) \\ M(x) \end{bmatrix} = \mathbf{Z}_R \begin{bmatrix} \dot{w}(x) \\ \dot{\theta}(x) \end{bmatrix} \quad (2.18)$$

where

$$\mathbf{Z}_R = \begin{bmatrix} (1+j)EI_{yy}k_b^3/\omega & -EI_{yy}k_b^2/\omega \\ EI_{yy}k_b^2/\omega & -(1-j)EI_{yy}k_b/\omega \end{bmatrix} \quad (2.19)$$

is the impedance matrix corresponding to an infinite end at the right hand end of the beam (Pan and Hansen, 1993b). Similarly, the wave impedance matrix corresponding to an infinite end at the left hand end of the beam is

$$\mathbf{Z}_L = \begin{bmatrix} -(1+j)EI_{yy}k_b^3/\omega & -EI_{yy}k_b^2/\omega \\ EI_{yy}k_b^2/\omega & (1-j)EI_{yy}k_b/\omega \end{bmatrix}. \quad (2.20)$$

2.2.2.3 Impedance equations

From Equation (2.9) the left hand boundary condition of the beam at $x = x_L$ can be written as

$$\begin{bmatrix} F(x_L) \\ M(x_L) \end{bmatrix} = \begin{bmatrix} Z_{Lf\dot{w}} & Z_{Lf\dot{\theta}} \\ Z_{Lm\dot{w}} & Z_{Lm\dot{\theta}} \end{bmatrix} \begin{bmatrix} \dot{w}_1(x_L) \\ \dot{\theta}_1(x_L) \end{bmatrix}. \quad (2.21)$$

Replacing the bending moment and shear force with a derivative of the displacement function, the following is obtained,

$$\begin{bmatrix} Z_{Lf\dot{w}} & Z_{Lf\dot{\theta}} \\ Z_{Lm\dot{w}} & Z_{Lm\dot{\theta}} \end{bmatrix} \begin{bmatrix} \dot{w}_1(x_L) \\ \dot{\theta}_1(x_L) \end{bmatrix} + EI_{yy} \begin{bmatrix} -w_1'''(x_L) \\ w_1''(x_L) \end{bmatrix} = 0. \quad (2.22)$$

Similarly, for the right hand end of the beam ($x = x_R$),

$$\begin{bmatrix} Z_{Rf\dot{w}} & Z_{Rf\dot{\theta}} \\ Z_{Rm\dot{w}} & Z_{Rm\dot{\theta}} \end{bmatrix} \begin{bmatrix} \dot{w}_2(x_R) \\ \dot{\theta}_2(x_R) \end{bmatrix} + EI_{yy} \begin{bmatrix} -w_2'''(x_R) \\ w_2''(x_R) \end{bmatrix} = 0. \quad (2.23)$$

Equations (2.3) and (2.4) may be differentiated to produce expressions for \dot{w}_1 , \dot{w}_2 , $\dot{\theta}_1$, $\dot{\theta}_2$, w_1' , w_1'' , w_1''' , w_2' , w_2'' and w_2''' , which can be substituted into Equations (2.22) and (2.23) to produce four boundary condition equations.

2.2.3 Equilibrium conditions at the point of application ($x = x_0$) of a force or moment

Requiring that the displacement and gradient be continuous at any point along the beam, the first two equilibrium conditions which must be satisfied at $x = x_0$ are

$$w_1 = w_2 \quad (2.24)$$

and

$$\frac{\partial w_1}{\partial x} = \frac{\partial w_2}{\partial x} . \quad (2.25)$$

The form of the excitation $q(x)$ will affect the higher order equilibrium conditions at $x = x_0$. In the following sections the equilibrium conditions corresponding to the beam excited by a point force and a concentrated moment acting about an axis parallel to the y -axis are discussed. These two types of excitation are induced by an actuator placed between a stiffener flange and the beam.

2.2.3.1 Response of a beam to a point force

To begin, $q(x)$ in Equation (2.1) is replaced by $q(x) = F_0\delta(x - x_0)$, where F_0 is the amplitude of a simple harmonic point force acting perpendicular to the beam at position x_0 and δ is the Dirac delta function. The first two boundary conditions at $x = x_0$ are given by Equations (2.24) and (2.25). The second and third order boundary conditions are obtained by twice integrating Equation (2.1) with respect to x between the limits $(x - x_0)$ and $(x + x_0)$:

Chapter 2. Control of vibrations in a stiffened beam

$$\frac{\partial^2 w_1}{\partial x^2} = \frac{\partial^2 w_2}{\partial x^2} \quad (2.26)$$

and

$$\frac{\partial^3 w_1}{\partial x^3} - \frac{\partial^3 w_2}{\partial x^3} = \frac{-F_0}{EI_{yy}} \quad (2.27)$$

2.2.3.2 Response of a beam to a concentrated moment

The excitation represented by $q(x)$ in Equation (2.1) is replaced by a concentrated moment M_0 acting at locations x_0 . The excitation $q(x)$ is replaced by $q(x) = \frac{\partial M_0}{\partial x} \delta(x - x_0)$. The second and third order boundary conditions at $x = x_0$ are

$$\frac{\partial^2 w_1}{\partial x^2} - \frac{\partial^2 w_2}{\partial x^2} = \frac{-M_0}{EI_{yy}} \quad (2.28)$$

and

$$\frac{\partial^3 w_1}{\partial x^3} = \frac{\partial^3 w_2}{\partial x^3} \quad (2.29)$$

Taking two boundary conditions at each end of the beam from Equations (2.22) and (2.23), the two equilibrium condition Equations (2.24) and (2.25), and two further equilibrium conditions from (2.26) - (2.29), there are eight equations in the eight unknowns $A_1, B_1, C_1,$

D_1, A_2, B_2, C_2 and D_2 . These can be written in the form $\alpha X = B$. The solution vectors $X = [A_1 \ B_1 \ C_1 \ D_1 \ A_2 \ B_2 \ C_2 \ D_2]^T = \alpha^{-1}B$ can be used to characterise the response of a beam to simple harmonic excitation by a point force or a concentrated moment.

2.2.4 Mass loading of the angle stiffener

The mass of the angle stiffener could be significant and may be taken into account as follows. Given a beam with an arbitrary excitation q at location $x = x_0$ and an angle stiffener at location $x = x_1$, as shown in Figure 2.4, three eigenfunction solutions of Equation (2.1) would be required; one applying over the range $x < x_0$, the second for $x_0 < x < x_1$, and the third applying when $x > x_1$.

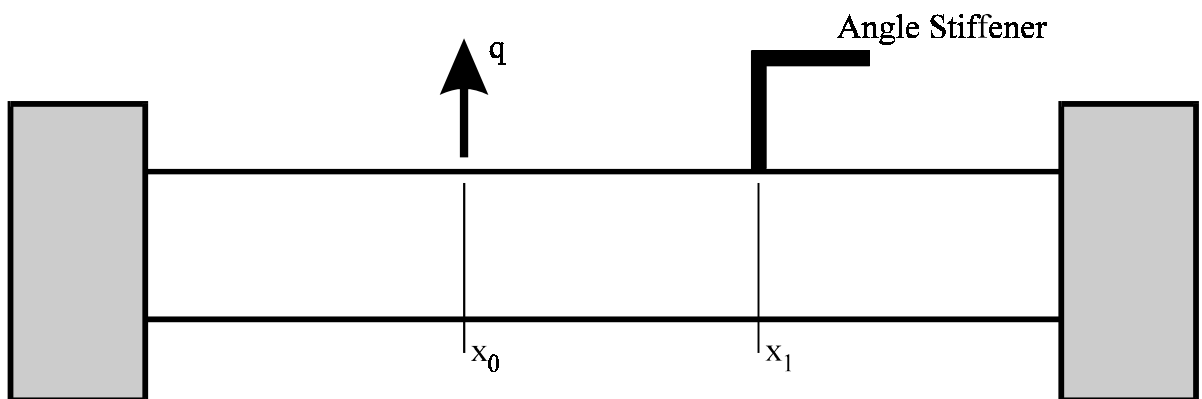


Figure 2.4 Beam with an excitation q and an angle stiffener.

Chapter 2. Control of vibrations in a stiffened beam

At the stiffener location $x = x_1$, the first two equilibrium conditions would be similar to Equations (2.24) and (2.25). The second and third order equilibrium equations would be

$$\frac{\partial^2 w_1}{\partial x^2} = \frac{\partial^2 w_2}{\partial x^2} \quad (2.30)$$

and

$$\frac{\partial^3 w_1}{\partial x^3} - \frac{\partial^3 w_2}{\partial x^3} = \frac{-m_a}{EI_{yy}} \frac{\partial^2 w}{\partial t^2}. \quad (2.31)$$

The beam used in experiments for this work was quite thick, and the mass loading of the stiffener made no measurable difference to the vibration response of the beam (see Section 2.4). The mass loading of the stiffener has therefore not been taken into account in this chapter; however, the effects of both the mass and the stiffness of the angle stiffener are considered in the chapters dealing with plates and cylinders (Chapters 3 and 4).

2.2.5 Minimising vibration using piezoceramic actuators and angle stiffeners

2.2.5.1 One control source and one angle stiffener

For any force or moment excitation, the eight boundary and equilibrium equations in eight unknowns can be written in the form $\alpha \mathbf{X} = \mathbf{B}$, where

$$\mathbf{B} = \mathbf{F} = \left[0, 0, 0, 0, 0, 0, 0, \frac{-F_0}{EI_{yy} k_b^3} \right]^T \quad (2.32)$$

for a force excitation and

$$\mathbf{B} = \mathbf{M} = \left[0, 0, 0, 0, 0, 0, \frac{-M_0}{EI_{yy}k_b^2}, 0 \right]^T \quad (2.33)$$

for a moment excitation. The coefficient matrix $\boldsymbol{\alpha}$ is given by Equation (2.34), where

$$\beta_L = e^{k_b x_L}, \beta_0 = e^{k_b x_0}, \beta_R = e^{k_b x_R}, \beta_L^j = e^{jk_b x_L}, \beta_0^j = e^{jk_b x_0}, \beta_R^j = e^{jk_b x_R}, Q_1 = \frac{EI_{yy}k_b^3}{j\omega} \text{ and } Q_2 = \frac{EI_{yy}k_b^2}{j\omega}.$$

Figure 2.5 shows the resultant forces and moments applied to the beam by the angle stiffener and piezoceramic stack (shown in Figure 2.1), with a primary force F_p at $x = x_p$. Control forces F_1 and F_2 act at $x = x_1$ and $x = x_2$ respectively, with the concentrated moment M_1 also acting at $x = x_1$. An error sensor is located at axial location $x = x_e$.

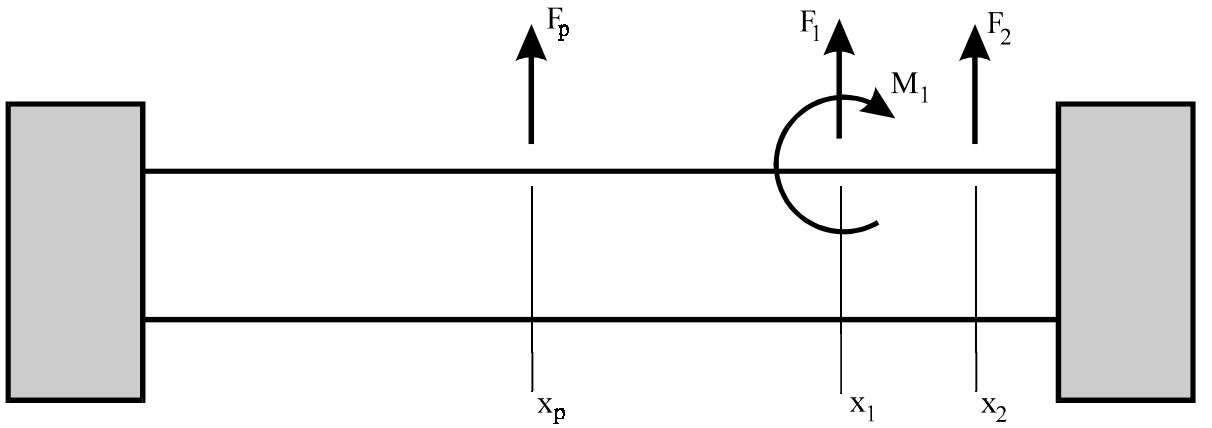


Figure 2.5 Forces and moment applied to the beam by a point force primary source and a piezoceramic stack and angle stiffener control source.

Chapter 2. Control of vibrations in a stiffened beam

$$\alpha = \begin{bmatrix}
 j\omega\beta_L(Z_{Lm\dot{w}} - k_b Z_{Lm\dot{\theta}} + Q_2) & \frac{j\omega(Z_{Lm\dot{w}} + k_b Z_{Lm\dot{\theta}} + Q_2)}{\beta_L} & j\omega\beta_L^j(Z_{Lm\dot{w}} - jk_b Z_{Lm\dot{\theta}} - Q_2) & \frac{j\omega(Z_{Lm\dot{w}} + jk_b Z_{Lm\dot{\theta}} - Q_2)}{\beta_L^j} \\
 j\omega\beta_L(Z_{Lf\dot{w}} - k_b Z_{Lf\dot{\theta}} - Q_1) & \frac{j\omega(Z_{Lf\dot{w}} + k_b Z_{Lf\dot{\theta}} + Q_1)}{\beta_L} & j\omega\beta_L^j(Z_{Lf\dot{w}} - jk_b Z_{Lf\dot{\theta}} + jQ_1) & \frac{j\omega(Z_{Lf\dot{w}} + jk_b Z_{Lf\dot{\theta}} - jQ_1)}{\beta_L^j} \\
 0 & 0 & 0 & 0 \\
 0 & 0 & 0 & 0 \\
 \beta_0 & 1/\beta_0 & \beta_0^j & 1/\beta_0^j \\
 \beta_0 & -1/\beta_0 & j\beta_0^j & -j/\beta_0^j \\
 \beta_0 & 1/\beta_0 & -\beta_0^j & -1/\beta_0^j \\
 -\beta_0 & 1/\beta_0 & j\beta_0^j & -j/\beta_0^j \\
 \\
 0 & 0 & 0 & 0 \\
 0 & 0 & 0 & 0 \\
 j\omega\beta_R(Z_{Rm\dot{w}} - k_b Z_{Rm\dot{\theta}} + Q_2) & \frac{j\omega(Z_{Rm\dot{w}} + k_b Z_{Rm\dot{\theta}} + Q_2)}{\beta_R} & j\omega\beta_R^j(Z_{Rm\dot{w}} - jk_b Z_{Rm\dot{\theta}} - Q_2) & \frac{j\omega(Z_{Rm\dot{w}} + jk_b Z_{Rm\dot{\theta}} - Q_2)}{\beta_R^j} \\
 j\omega\beta_R(Z_{Rf\dot{w}} - k_b Z_{Rf\dot{\theta}} - Q_1) & \frac{j\omega(Z_{Rf\dot{w}} + k_b Z_{Rf\dot{\theta}} + Q_1)}{\beta_R} & j\omega\beta_R^j(Z_{Rf\dot{w}} - jk_b Z_{Rf\dot{\theta}} + jQ_1) & \frac{j\omega(Z_{Rf\dot{w}} + jk_b Z_{Rf\dot{\theta}} - jQ_1)}{\beta_R^j} \\
 -\beta_0 & -1/\beta_0 & -\beta_0^j & -1/\beta_0^j \\
 -\beta_0 & 1/\beta_0 & -j\beta_0^j & j/\beta_0^j \\
 -\beta_0 & -1/\beta_0 & \beta_0^j & 1/\beta_0^j \\
 \beta_0 & -1/\beta_0 & -j\beta_0^j & j/\beta_0^j
 \end{bmatrix}, \tag{2.34}$$

Chapter 2. Control of vibrations in a stiffened beam

The equation in the displacement unknowns for the primary (excitation) point force is

$$\boldsymbol{\alpha}_p \mathbf{X}_p = \mathbf{F}_p , \quad (2.35)$$

or

$$\mathbf{X}_p = \boldsymbol{\alpha}_p^{-1} \mathbf{F}_p , \quad (2.36)$$

where \mathbf{F}_p is defined by Equation (2.32) with $F_0 = F_p$, $\boldsymbol{\alpha}_p$ is the matrix of boundary condition coefficients for the primary force and \mathbf{X}_p is the boundary eigenvector for the primary force.

Similarly

$$\mathbf{X}_1 = \boldsymbol{\alpha}_1^{-1} \mathbf{F}_1 \quad (2.37)$$

and

$$\mathbf{X}_2 = \boldsymbol{\alpha}_2^{-1} \mathbf{F}_2 , \quad (2.38)$$

where \mathbf{X}_1 and \mathbf{X}_2 are the boundary eigenvectors for the two control forces. In addition,

$$\mathbf{X}_m = \boldsymbol{\alpha}_m^{-1} \mathbf{M} , \quad (2.39)$$

where \mathbf{X}_m is the boundary eigenvector for the control moment and \mathbf{M} is defined by Equation (2.33). At the error sensor ($x = x_e$), the displacement due to each force and the moment is given by, for $z = p, 1, 2$ and m ,

$$w_z(x_e) = \mathbf{X}_z^T \mathbf{E}(x_e) , \quad (2.40)$$

Chapter 2. Control of vibrations in a stiffened beam

where \mathbf{X}^T indicates the transpose of the matrix \mathbf{X} and

$$\mathbf{E}(x_e) = \begin{bmatrix} 0 \\ 0 \\ 0 \\ 0 \\ e^{k_b x_e} \\ e^{-k_b x_e} \\ e^{jk_b x_e} \\ e^{-jk_b x_e} \end{bmatrix}. \quad (2.41)$$

By summation of the displacement equations (Equation (2.40)), the total displacement resulting from the primary and control excitations is

$$\begin{aligned} w(x_e) &= w_p(x_e) + w_1(x_e) + w_2(x_e) + w_m(x_e) \\ &= \mathbf{X}_p^T \mathbf{E}(x_e) + \mathbf{X}_1^T \mathbf{E}(x_e) + \mathbf{X}_2^T \mathbf{E}(x_e) + \mathbf{X}_m^T \mathbf{E}(x_e). \end{aligned} \quad (2.42)$$

Substituting Equations (2.36) - (2.39) into (2.42),

$$\begin{aligned} w(x_e) &= (\boldsymbol{\alpha}_p^{-1} \mathbf{F}_p)^T \mathbf{E}(x_e) + (\boldsymbol{\alpha}_1^{-1} \mathbf{F}_1)^T \mathbf{E}(x_e) + (\boldsymbol{\alpha}_2^{-1} \mathbf{F}_2)^T \mathbf{E}(x_e) + (\boldsymbol{\alpha}_m^{-1} \mathbf{M})^T \mathbf{E}(x_e) \\ &= \frac{F_p}{k_b^3 EI_{yy}} (\boldsymbol{\alpha}_p^{-1})_{i,8}^T \mathbf{E}(x_e) + \frac{F_1}{k_b^3 EI_{yy}} (\boldsymbol{\alpha}_1^{-1})_{i,8}^T \mathbf{E}(x_e) \\ &\quad + \frac{F_2}{k_b^3 EI_{yy}} (\boldsymbol{\alpha}_2^{-1})_{i,8}^T \mathbf{E}(x_e) - \frac{M_1}{k_b^2 EI_{yy}} (\boldsymbol{\alpha}_m^{-1})_{i,7}^T \mathbf{E}(x_e). \end{aligned} \quad (2.43)$$

Defining the transpose of the eighth column of the inverse of $\boldsymbol{\alpha}_p$ as $\mathbf{P} = (\boldsymbol{\alpha}_p^{-1})_{i,8}^T$ (and similarly for $\mathbf{A} = (\boldsymbol{\alpha}_1^{-1})_{i,8}^T$, $\mathbf{B} = (\boldsymbol{\alpha}_2^{-1})_{i,8}^T$, and $\mathbf{C} = (\boldsymbol{\alpha}_m^{-1})_{i,7}^T$ is the transpose of the seventh

Chapter 2. Control of vibrations in a stiffened beam

column of the inverse of α_m), and setting $w(x_e) = 0$ to find the optimal control force,

Equation (2.43) can be re-written as

$$-AE(x_e)F_1 - BE(x_e)F_2 + k_b CE(x_e)M_1 = PE(x_e)F_p . \quad (2.44)$$

Analysis of the forces applied by the stack and angle stiffener gives $F_1 = -F_2 = F_s$ and $M_1 = -aF_s$, where F_s is the force applied by the piezoceramic stack (Figure 2.6) and is positive as shown.

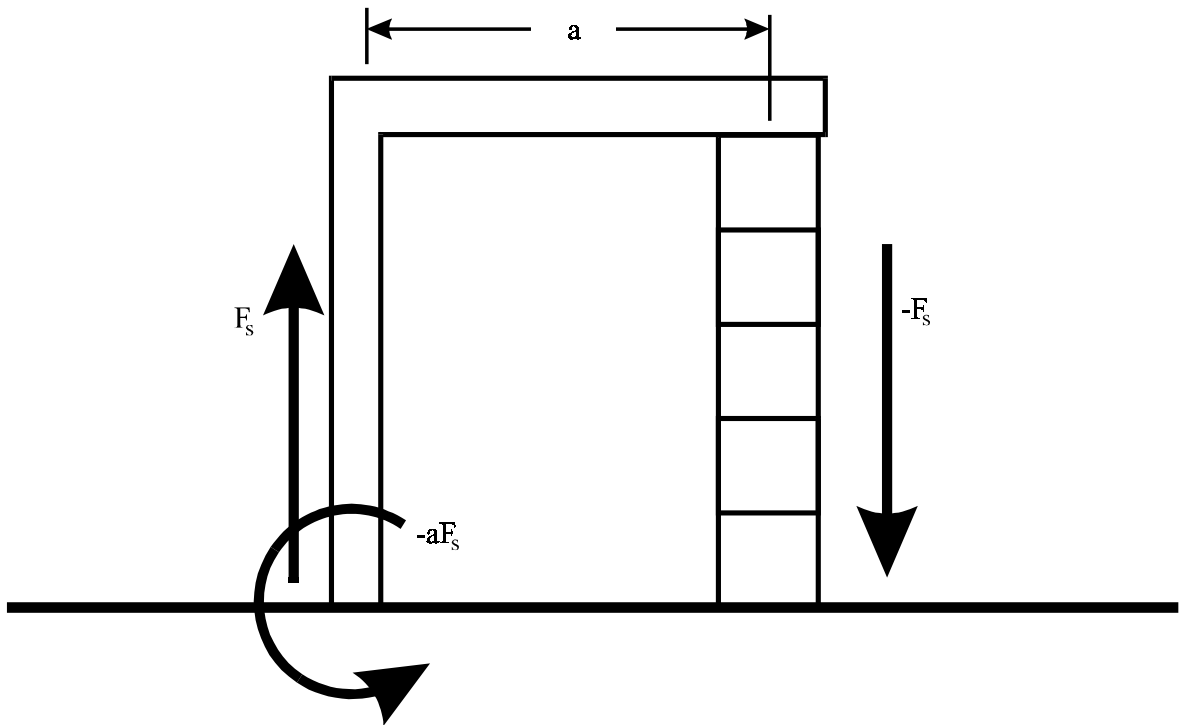


Figure 2.6 Control forces and moment in terms of piezoceramic stack force F_s .

Substituting these quantities into Equation (2.44), the optimal control force F_s can be written

Chapter 2. Control of vibrations in a stiffened beam

as

$$F_s = \frac{PE(x_e)}{BE(x_e) - AE(x_e) - k_b a C E(x_e)} F_p, \quad (2.45)$$

or

$$F_s = \frac{PE(x_e)}{(B - A - k_b a C) E(x_e)} F_p. \quad (2.46)$$

2.2.5.2 Two control sources and two angle stiffeners

If a second control source and angle stiffener are introduced at some location x_c' downstream from the first, Equation (2.42) becomes

$$w(x_e) = w_p(x_e) + w_1(x_e) + w_2(x_e) + w_m(x_e) + w_1'(x_e) + w_2'(x_e) + w_m'(x_e) = \mathbf{X}_p^T \mathbf{E}(x_e) + \mathbf{X}_1^T \mathbf{E}(x_e) + \mathbf{X}_2^T \mathbf{E}(x_e) + \mathbf{X}_m^T \mathbf{E}(x_e) + \mathbf{X}_1'^T \mathbf{E}(x_e) + \mathbf{X}_2'^T \mathbf{E}(x_e) + \mathbf{X}_m'^T \mathbf{E}(x_e), \quad (2.47)$$

where the prime refers to the values associated with the second control source. The control signal for the second source required to minimise vibration at the same error sensor location x_e can be calculated by

$$F_s' = \frac{PE(x_e)F_p - (B - A - k_b a C)E(x_e)F_s}{(B' - A' - k_b a C')E(x_e)}. \quad (2.48)$$

In this way, the magnitude of the first control source signal can be limited to some arbitrary maximum value, and the second control source used to maintain optimal control.

2.2.5.3 Two error sensors

If a second error sensor is introduced at some location x_e' downstream from the first, and a single control source driven in an attempt to optimally reduce vibration at both locations, Equation (2.42) becomes

$$w(x_e) = \mathbf{X}_p^T [\mathbf{E}(x_e) + \mathbf{E}(x_e')] + \mathbf{X}_1^T [\mathbf{E}(x_e) + \mathbf{E}(x_e')] + \mathbf{X}_2^T [\mathbf{E}(x_e) + \mathbf{E}(x_e')] + \mathbf{X}_m^T [\mathbf{E}(x_e) + \mathbf{E}(x_e')] \quad (2.49)$$

This has the effect of shifting the effective error sensor location to some location between x_e and x_e' . No improvement in overall attenuation is achieved.

An alternative method of utilising a second error sensor would be to introduce the second sensor only when control using the first error sensor was ineffective (see Section 2.3.3). However, this would be a difficult method to implement in practice. Unlike the case where the control source is badly located (see Section 2.3.2), there is no effect on the control source amplitude required to give optimal control when the error sensor is badly located. The only observed effect is a decrease in the attenuation achieved. To use a second error sensor when the frequency of excitation resulted in the first error sensor location being unsuitable would require some method of measuring the reduction in acceleration level achieved downstream from the first error sensor. When the reduction was less than some expected level, the

Chapter 2. Control of vibrations in a stiffened beam

controller would be switched to use the second error sensor. This method is not useful because it requires the addition of even more sensors, and there is no more practical way of determining when a second error sensor should be used in preference to the first. Use of a second error sensor downstream from the first would yield no practical benefit.

2.3 NUMERICAL RESULTS

The theoretical model developed in the previous section was programmed in Fortran. The program consisted of about 1000 lines and, for a typical set of results, took two or three hours C.P.U. time to run on a DEC 5000/240 computer.

The discussion that follows examines the effect of varying forcing frequency, control source location (which is defined here as the location of the angle-beam joint), error sensor location, and stiffener flange length on the active control of vibration in beams with four sets of end conditions; infinite, fixed, free and simply supported. The beam parameters (including location of the control source, primary source and error sensor) are listed in Table 2.2. These values are adhered to unless otherwise stated. The results obtained are consistent with previous work done by Pan and Hansen (1993a) for the case of a single point force harmonically applied to a beam and the analogous case of active noise control of ducts (Snyder 1990).

Control forces are expressed as a multiple of the primary force, and the acceleration amplitude dB scale reference level is the far field uncontrolled infinite beam acceleration produced by the primary force. In all cases, the control force is assumed to be optimally adjusted to minimise the acceleration at the error sensor location. The flexural wavelength of vibration in a beam is given by

$$\lambda_b = \frac{2\pi}{k_b} . \quad (2.50)$$

Table 2.2
Beam Parameters for Numerical Results

Parameter	Value
Beam length L_x	10.0 m
Beam width L_y	0.05 m
Beam height L_z	0.025 m
Young's modulus E	71.1 GPa
Primary force location x_p	0.0 m
Control location x_1	1.0 m $(2.07\lambda_b)^*$
Stiffener flange length a	0.05 m
Error sensor location x_e	2.0 m $(4.14\lambda_b)^*$
Frequency f	1000 Hz
Wavelength λ_b	0.4824 m*

* - Applies only when $f = 1000$ Hz.

2.3.1 Acceleration distributions for controlled and uncontrolled cases

Figure 2.7 shows the acceleration amplitude distribution in dB for the uncontrolled beams. The shape of the curve for the infinite beam represents a travelling wave field with an additional decaying evanescent field close to the source. For the beams not terminated anechoically, waves reflected from the ends of the beam cause a standing wave field to exist. It can be seen from the nature of the response that the near field effects become insignificant at less than one wavelength from the point of application of the primary force. Figure 2.8 shows the acceleration amplitude distribution for controlled cases, using the control, primary

Chapter 2. Control of vibrations in a stiffened beam

and error sensor locations given in Table 2.2. These locations are marked x_p , x_c and x_e respectively on the infinite beam curve. As expected, the curves for the controlled cases (Figure 2.8) dip to a minimum at the error sensor location ($x_e = 4.14\lambda_b$) where acceleration has been minimised. In all cases, the calculated reduction in acceleration amplitude downstream of the error sensor is over 100 dB. The reduction or increase in acceleration amplitude upstream of the primary force depends on the control source location, as discussed below.

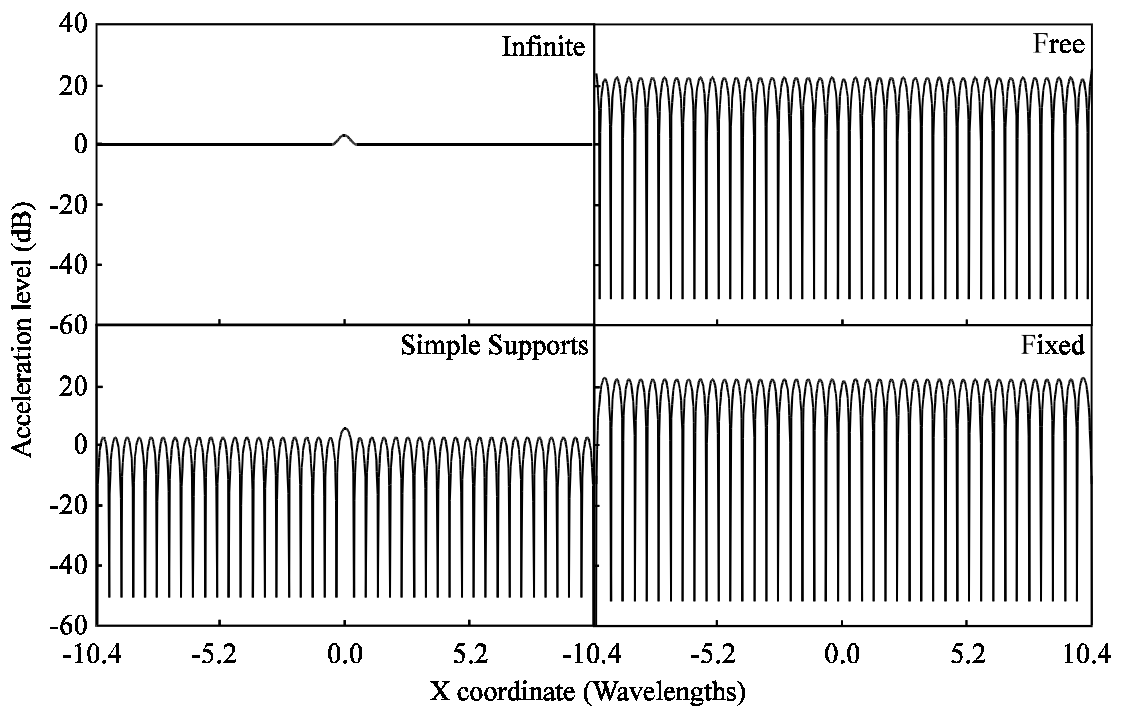


Figure 2.7 Acceleration distributions for the uncontrolled cases.

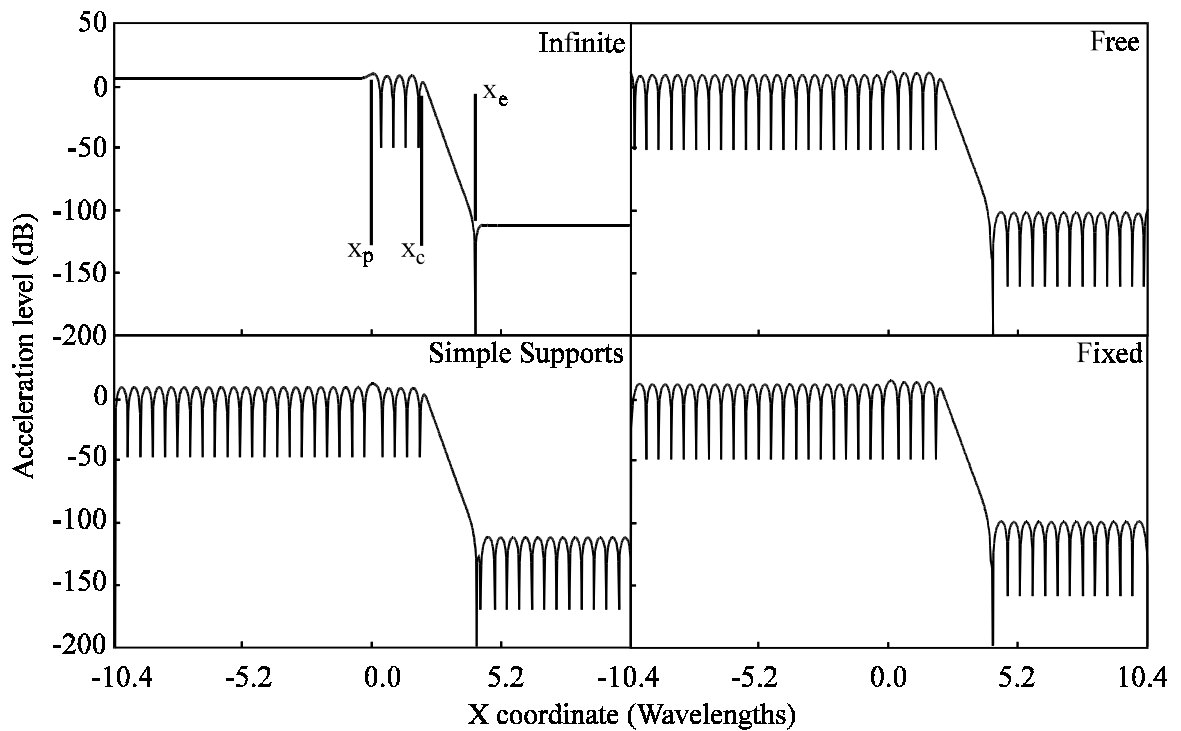


Figure 2.8 Acceleration distributions for the controlled cases.

2.3.2 Effect of variations in forcing frequency, stiffener flange length and control source location on the control force

Figure 2.9 shows the effect of varying the forcing frequency on the magnitude of the control force required to minimise the beam vibration at the error sensor location. The control source is located 1 metre from the primary source and the error sensor 2 metres from the primary source (Table 2.2).

The minima on the curves for fixed, free and simply supported beams occur at resonance frequencies, when control is easier (Pan *et al*, 1992). At these frequencies the control force amplitude becomes small but not zero. The maxima in Figure 2.9 occur when the relative spacing between primary and control sources is given by $x = (c + n\lambda_p/2)$ for integer n and

constant c . This effect is illustrated by Figure 2.10 which shows the control force amplitude as a function of separation between primary and control sources, with a constant error sensor location - control source separation of 1 metre ($2.07\lambda_b$).

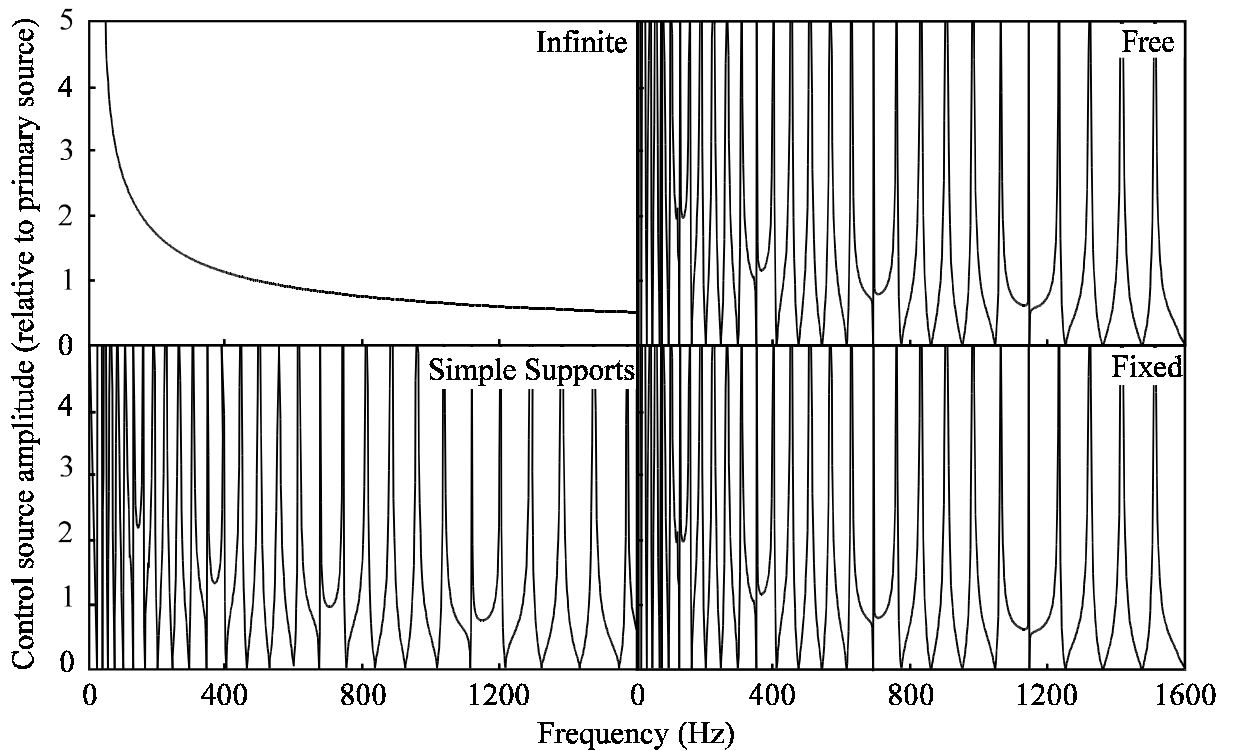


Figure 2.9 Control force amplitude for optimal control as a function of frequency.

The maxima occur because of the difficulty in controlling the flexural vibration when the effective control source location is at a node of the standing wave caused by reflection from the terminations. The constant c represents the distance (in wavelengths) between the primary source and the first node in the standing wave in the direction of the control source. This constant changes with frequency and termination type. For the fixed and free support beams, at $f = 1000$ Hz, c is approximately zero. Note that the effective control location is somewhere between the beam-angle connection and the actuator, and represents the location

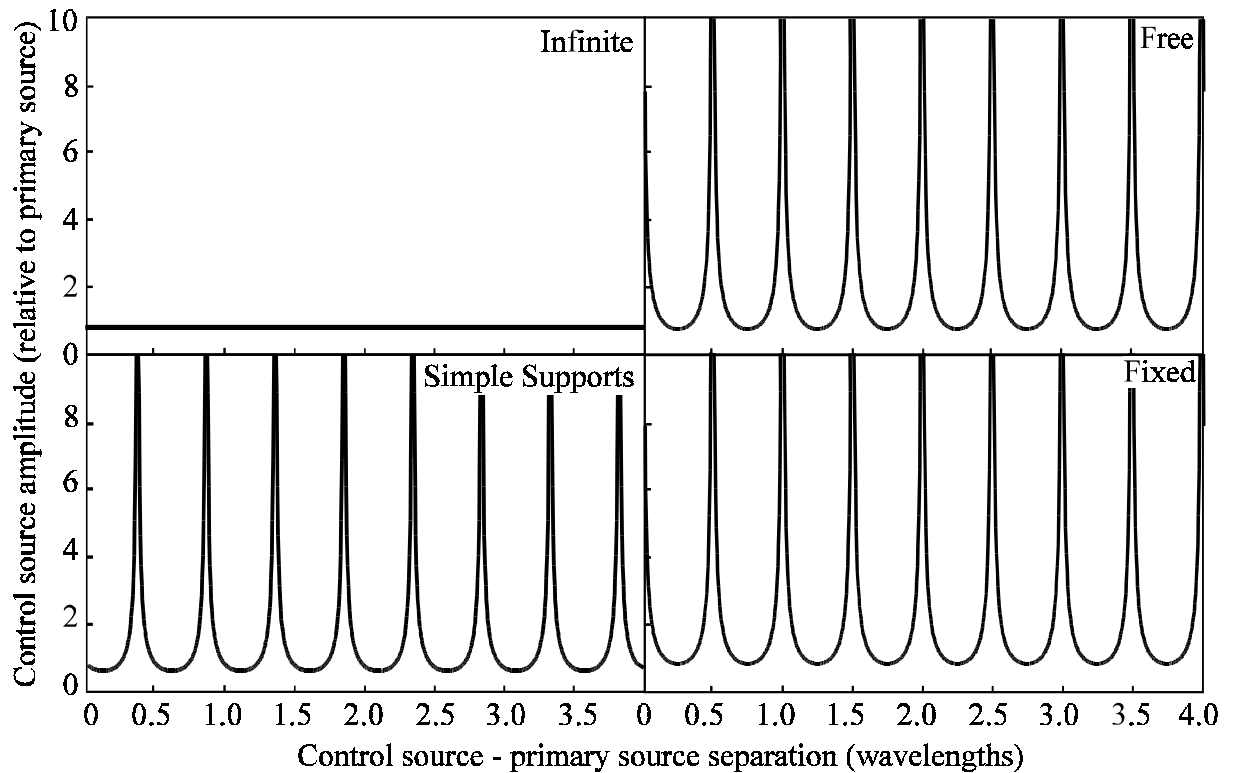


Figure 2.10 Control force amplitude for optimal control as a function of control location.

of the combined effect of the two forces and the moment as discussed.

Figure 2.11 shows the phase of the control source relative to the primary source as a function of frequency, again using the control, primary and error sensor locations given in Table 2.2. Apart from the infinite beam case, the control source is either in phase or 180° out of phase with the primary source, and this holds for all locations of control source, error sensor and all angle sizes. In the case of the infinite beam, the phase cycles through 180° with increasing frequency. The difference is due to the formation of standing waves on beams with end conditions other than infinite. When a standing wave is formed because of the reflection from the beam termination, the vibration, and hence the required control force, is in phase

with the excitation.

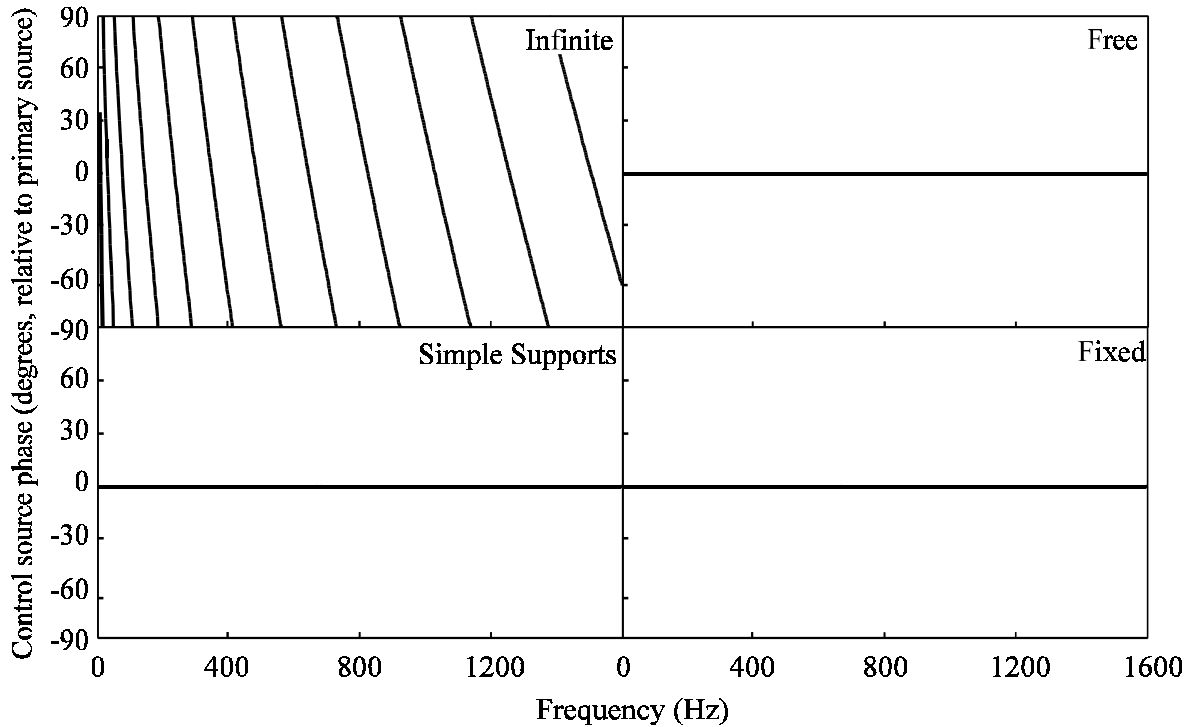


Figure 2.11 Control force phase for optimal control as a function of control location.

Figure 2.12 shows the control force amplitude plotted as a function of increasing stiffener flange length in wavelengths a/λ_b (see Figure 2.6 for definition of stiffener flange length). The exponential decrease in control force magnitude with increasing stiffener flange length can be attributed to the increasing size of the angle relative to the flexural wavelength. When the wavelength is large compared to the stiffener flange length, the two control forces operating in opposite directions tend to cancel. The exponential decrease in control force amplitude with increasing stiffener flange length can also be seen in Figure 2.9 where the relative control force amplitude is plotted as a function of frequency. As the excitation frequency increases, the stiffener flange length relative to the flexural wavelength increases,

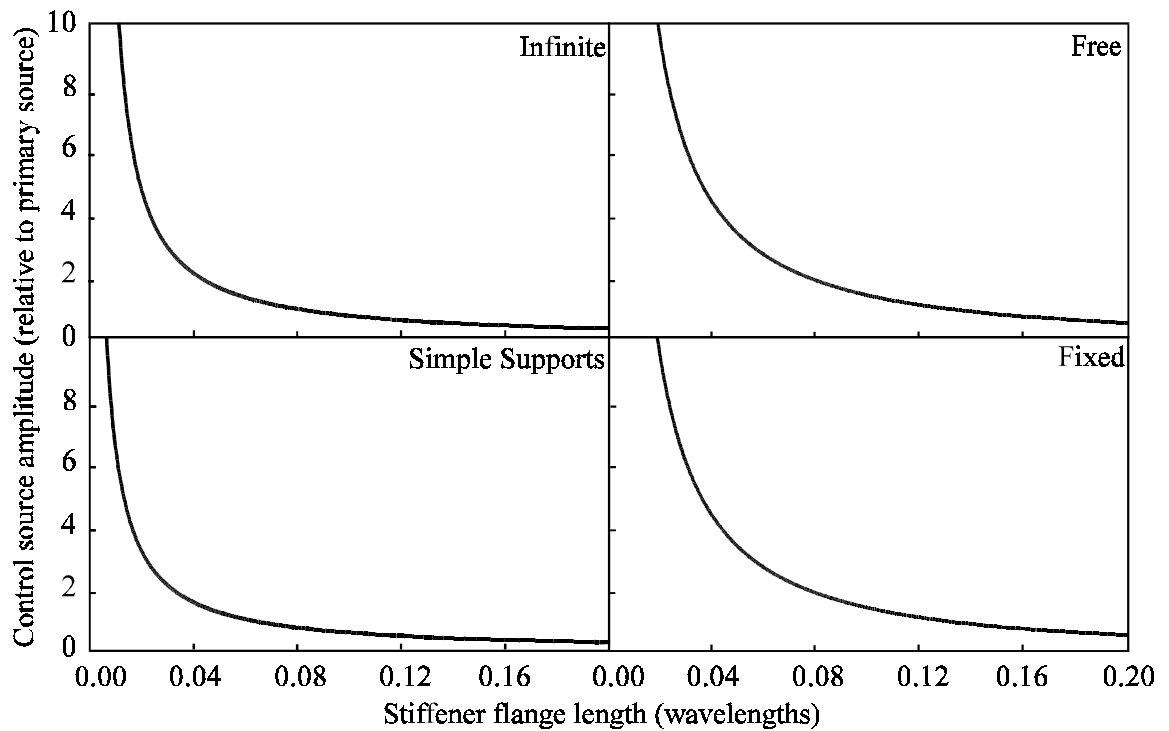


Figure 2.12 Control force amplitude for optimal control as a function of flange length.

and the control force amplitude decreases. It is difficult to see this effect on the fixed, free and simply supported case figures because of the super-position of the peaks and troughs, but at the frequencies where the peaks and troughs almost coincide (e.g. at 1150 Hz on the free beam figure) some flattening out of the curve is seen. The effect is much clearer on the infinite beam curve where the peaks and troughs are absent.

2.3.3 Effect of variations in forcing frequency, control source location and error sensor location on the attenuation of acceleration level

Figure 2.13 shows the variation in the mean attenuation of acceleration level upstream of the primary source for each beam as a function of the excitation frequency, and Figure 2.14 gives the corresponding results for mean attenuation of acceleration level downstream of the error sensor.

Figure 2.15 shows the variation in the mean attenuation of acceleration level upstream of the primary source for each beam as a function of separation between the primary and control sources. The separation between the error sensor location and the control source location is constant ($2.07\lambda_b$). The minima in the attenuation curve for the free, fixed and simply supported beams correspond to control source locations where maxima in the control force curve occur (Figure 2.10). Maximum attenuation is achieved in all cases with a control source - primary source separation of $(0.23 + n\lambda_b/2)$. This value is independent of the beam length and the excitation frequency. Noting also that the maxima occur for the infinite beam as well as the finite beams, it may be concluded that the maxima are a result of the standing wave field established between the primary and control sources only. This standing wave is present for the infinite beam case as well as the other terminations (see Figure 2.8). The effective control location is to the right of the defined control source location (which is the position of the stiffener-beam joint), so the effective control source-primary source separation giving these maxima is about $(0.25 + n\lambda_b/2)$. This result is consistent with analogous cases; for a beam excited by point forces only (Pan and Hansen, 1993a), and also for sound fields in ducts (Snyder, 1990).

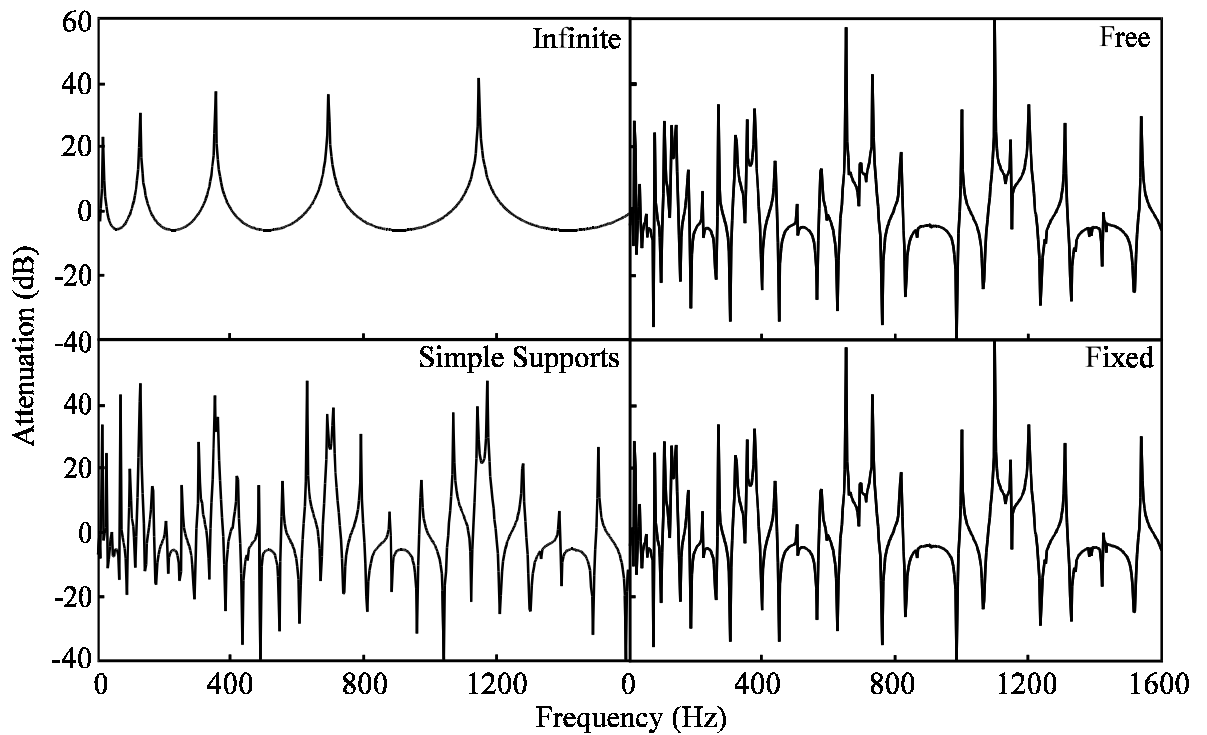


Figure 2.13 Mean attenuation upstream of the primary source as a function of frequency.

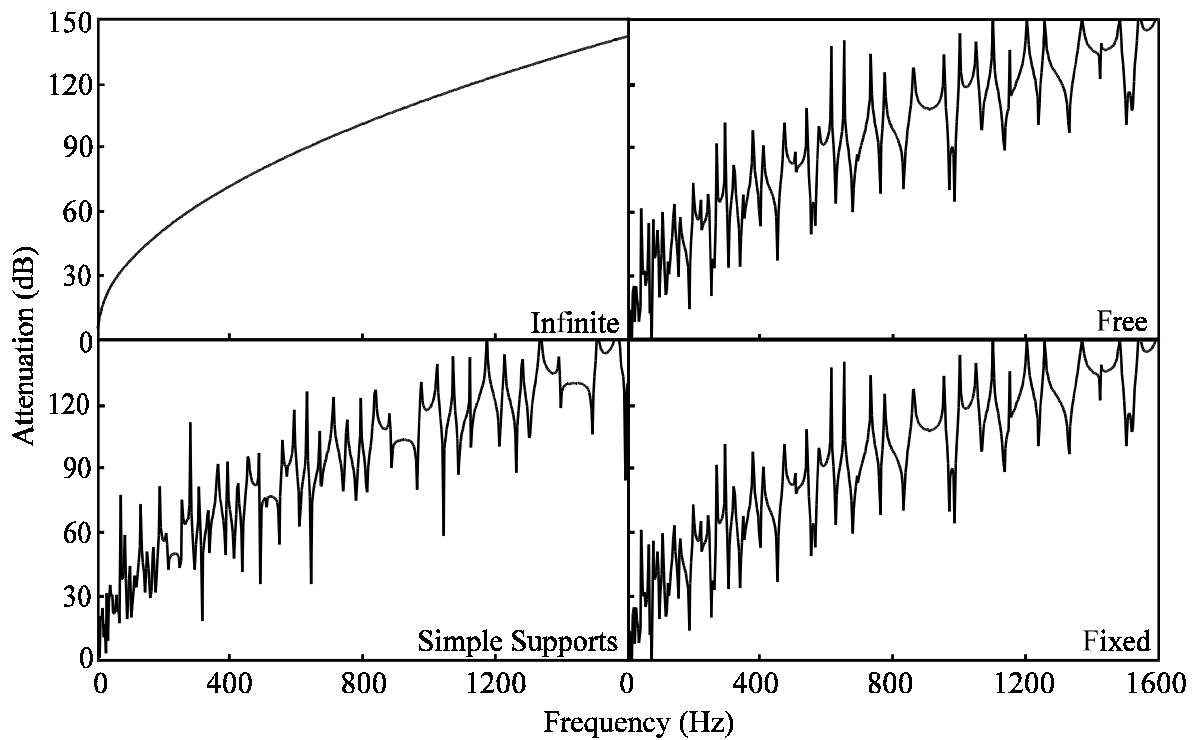


Figure 2.14 Mean attenuation downstream of the error sensor as a function of frequency.

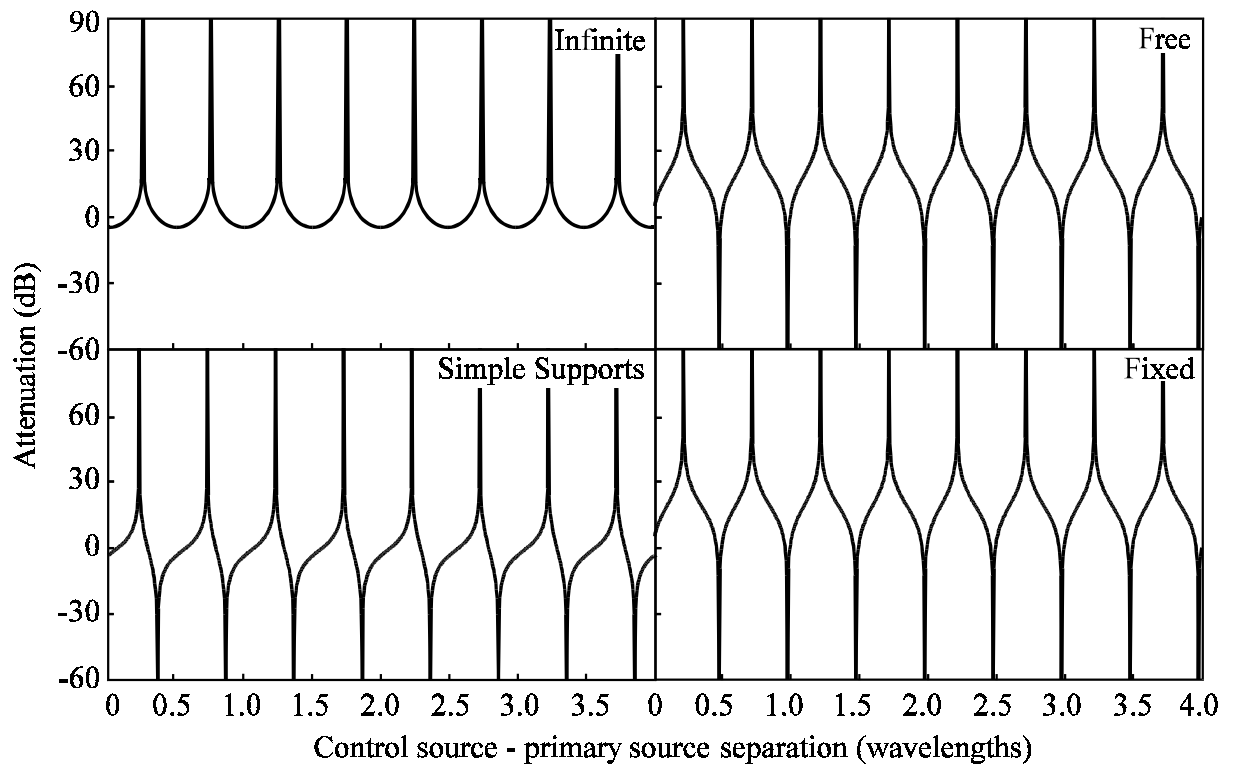


Figure 2.15 Mean attenuation upstream of the primary source as a function of control source - primary source separation.

Figure 2.16 shows the mean attenuation of acceleration level downstream of the error sensor as a function of separation between primary and control sources. The control source locations giving the best results upstream of the primary source also give high attenuation downstream of the error sensor. Every second minimum occurs at a location corresponding to a maximum in the control force curve (see Figure 2.10), and again these are separated by half a wavelength. Thus it may be concluded that the best attenuation is achieved when the control effort is a minimum. The additional minima occur at control source-primary source separations of $(d + n\lambda_b/2)$, where d is a constant dependent on frequency and termination type.

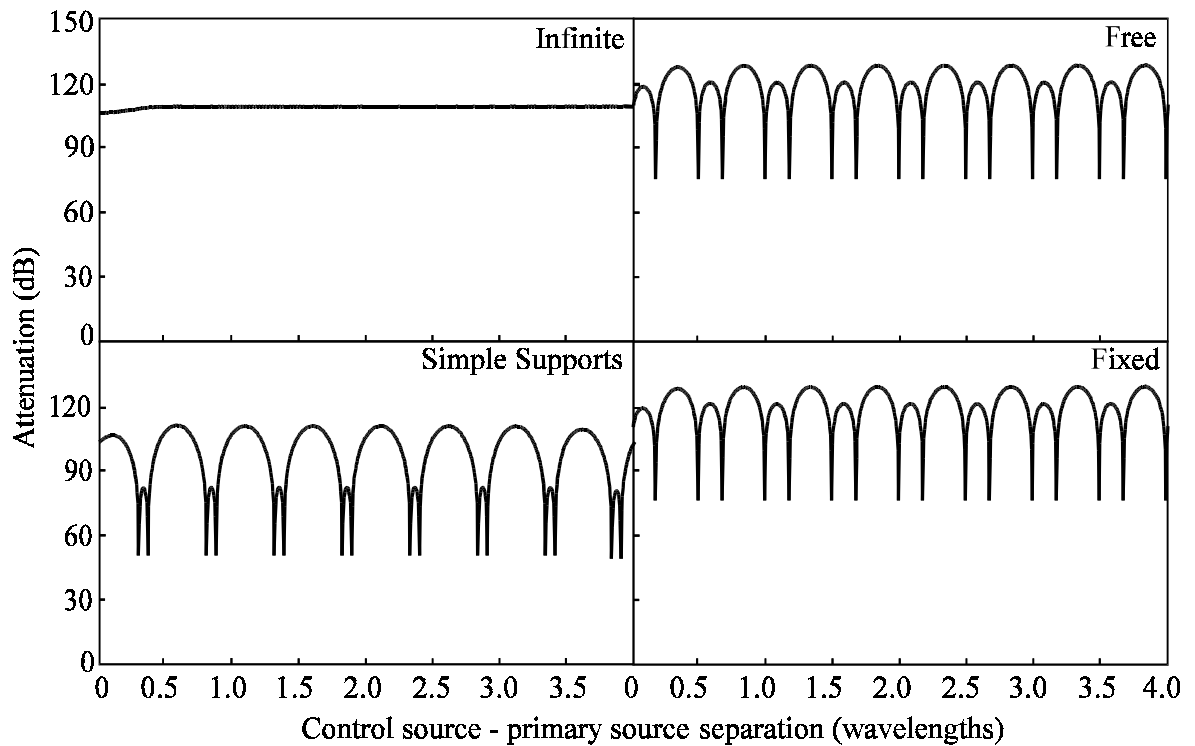


Figure 2.16 Mean attenuation downstream of the error sensor as a function of control source - primary source separation.

Figures 2.17 and 2.18 show the mean attenuation upstream of the primary source and downstream of the error sensor respectively as a function of the separation between the control source and error sensor. There is no change in the attenuation upstream of the control source with changing error sensor location outside of the control source near field (i.e. for separations between the control source and error sensor of over $0.75\lambda_b$). Downstream of the error sensor, mean attenuation increases with increasing separation between the error sensor and control source location at the rate of around 50 dB per wavelength separation. The minima in the curves for fixed, free and simply supported beams correspond to separations in the error sensor and control source location of $(d+n\lambda_b/2)$, where d is the constant dependent on frequency and termination type previously defined. The dips in the curves are represented correctly in the figures; finer frequency resolution would not cause them to be significantly lower.

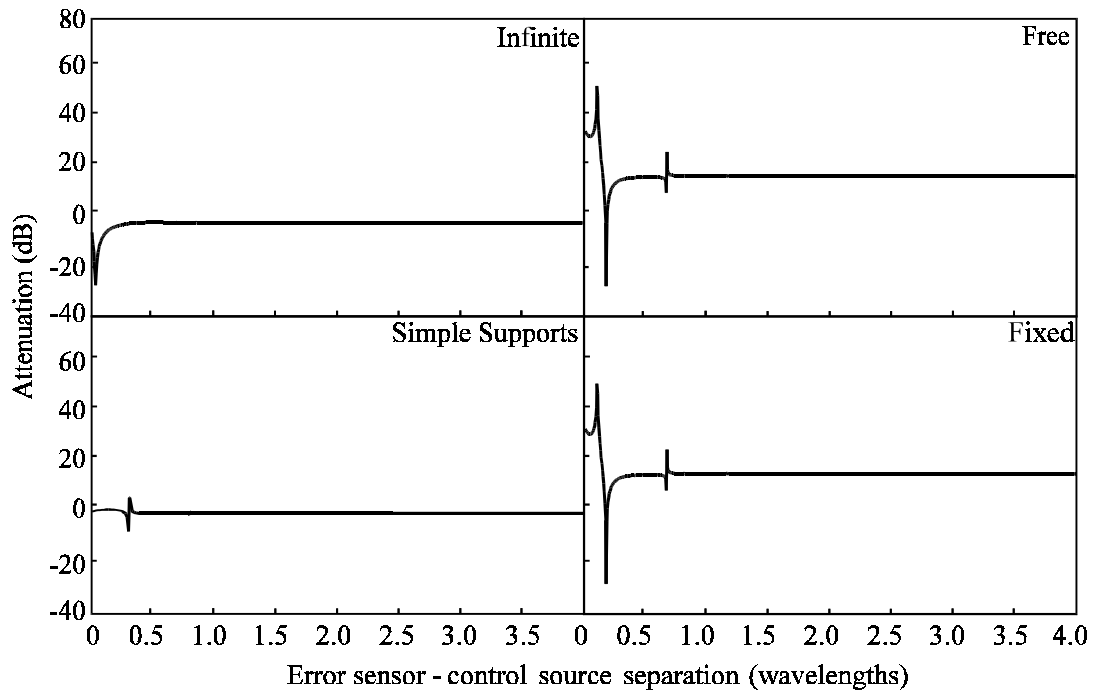


Figure 2.17 Mean attenuation upstream of the primary source as a function of error sensor - control source separation.

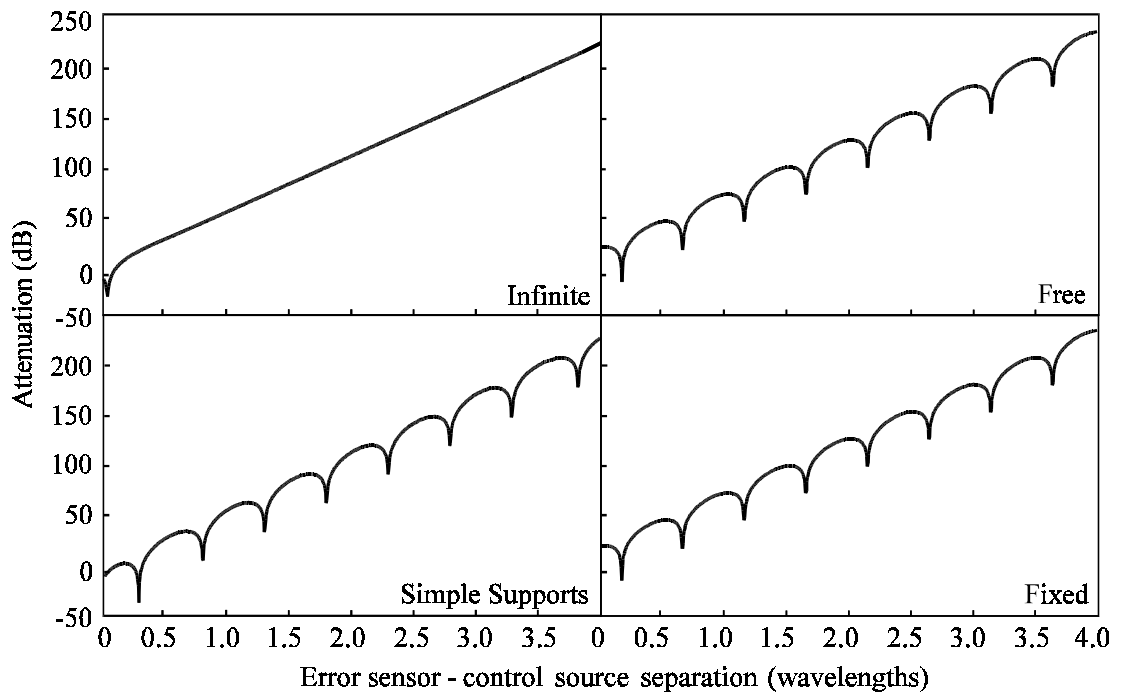


Figure 2.18 Mean attenuation downstream of the error sensor as a function of error sensor - control source separation.

2.3.4 Effect of a second angle stiffener and control source on the attenuation of acceleration level.

The results given in Section 2.3.3 indicate that there are some control source locations where significantly less attenuation can be achieved. Figure 2.19 shows the variation in amplitudes of two control sources driven to optimally control vibration at a single error sensor, as a function of control source location, at an excitation frequency of 1000 Hz. The first control source amplitude is limited to 1.5 times the primary source amplitude, and the second control source amplitude and phase calculated by the method given in Section 2.2.5.2. The second control source is located 0.15m downstream from the first, and the error sensor is located 1.0m downstream from the first control source. The control source amplitude for a single control source is also shown on Figure 2.19 for comparison. At this frequency, there are no control source locations at which control using the two control sources requires large control signals.

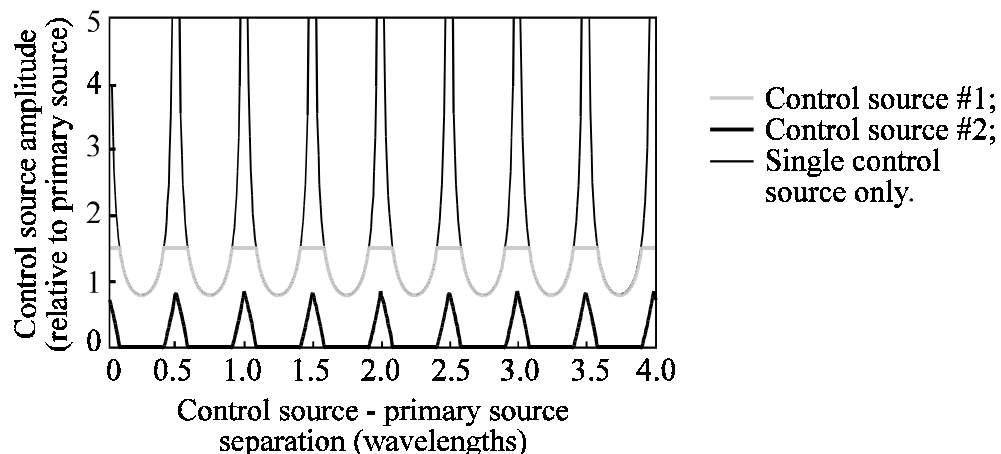


Figure 2.19 Control source amplitudes for one and two control sources as a function of control source - primary source separation for the beam with fixed ends.

Chapter 2. Control of vibrations in a stiffened beam

Figure 2.20 gives the control source amplitudes for two control sources as a function of frequency. It can be seen that there are some lower frequencies where the amplitude of the second control source required for optimal control is high. This can be overcome by using a different spacing between the first and second control sources.

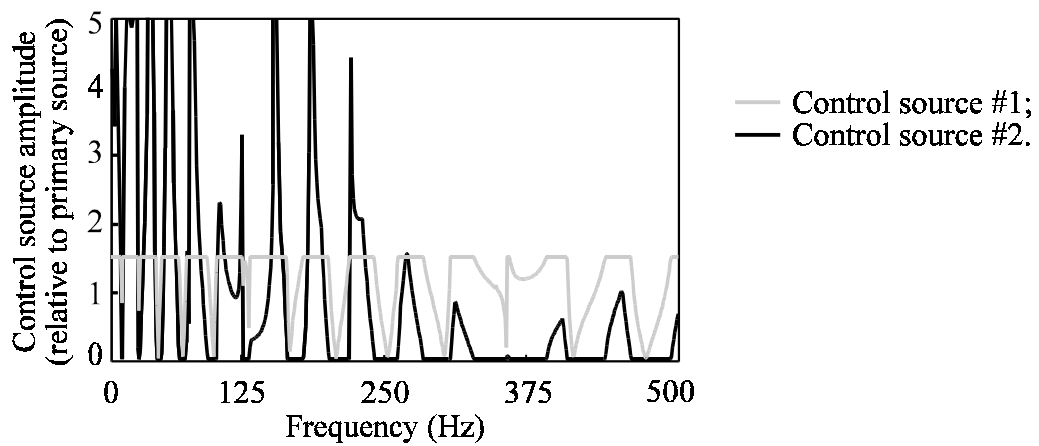


Figure 2.20 Control source amplitudes for two control sources as a function of frequency for the beam with fixed ends for the beam with fixed ends.

Figure 2.21 shows that the minima in attenuation upstream of the primary sources observed at half-wavelength intervals in control source - primary source separation using one control source only are eliminated by the introduction of the second control source. When the location of a single control source is such that a large control signal is required to control vibration at the error sensor, the vibration level upstream of the primary source is increased severely. As these large control signals are not required when two control sources are used (Figure 2.19), this problem is overcome. The corresponding minima in attenuation downstream of the error sensors are also eliminated by the introduction of the second control

Chapter 2. Control of vibrations in a stiffened beam

source (Figure 2.22). The minima that remain when using two control sources (at control source - primary source separations given by $(d + n\lambda_p/2)$, where d is the constant defined in Section 2.3.3, are a consequence of the error sensor location and cannot be overcome simply. The difficulties involved in effectively introducing a second error sensor downstream from the first are discussed in Section 2.2.5.3.

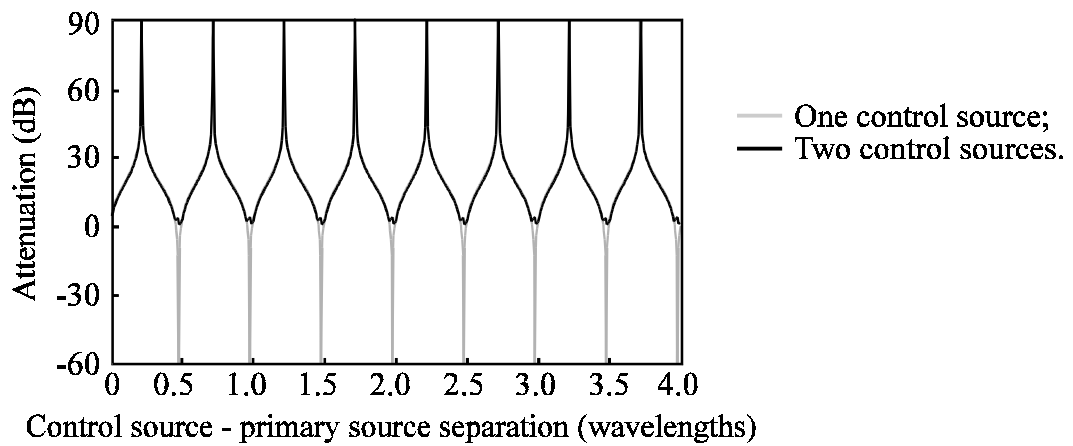


Figure 2.21 Mean attenuation upstream of the primary source as a function of control location for the beam with fixed ends.

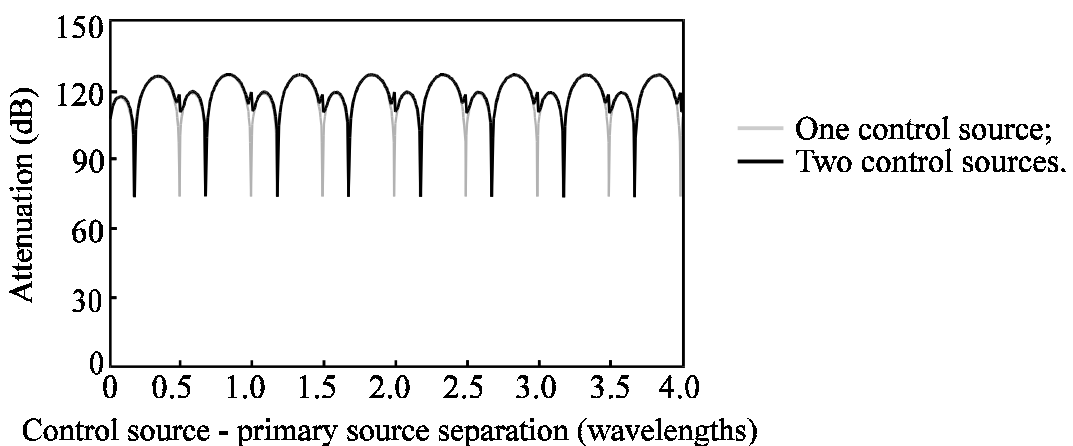


Figure 2.22 Mean attenuation downstream of the error sensor as a function of control location for the beam with fixed ends.

2.4 EXPERIMENTAL PROCEDURE

2.4.1 Impedance of an experimental termination

Before experimental results and theoretical calculations can be compared, it is necessary to know the impedance of the beam termination used in the experiment. Traditionally, classical terminations (such as the "free end") have been used in theoretical work, and modelled experimentally (e.g. by wire supports). For greater accuracy, the impedances used in the theoretical results that follow were calculated using a method similar to that developed by Fuller *et al* (1990), except that coupling impedances are initially included in the analysis.

Beam end conditions may be characterised by impedance matrices \mathbf{Z}_L and \mathbf{Z}_R corresponding respectively to the left and right ends of the beam (see Section 2.2.2.1);

$$\mathbf{Z}_L = \begin{bmatrix} Z_{Lf\dot{w}} & Z_{Lf\dot{\theta}} \\ Z_{Lm\dot{w}} & Z_{Lm\dot{\theta}} \end{bmatrix} = \begin{bmatrix} \frac{1}{Z_{Lf}} & \frac{1}{Z_{Lfm}} \\ \frac{1}{Z_{Lmf}} & \frac{1}{Z_{Lm}} \end{bmatrix}^{-1} \quad (2.51)$$

and

$$\mathbf{Z}_R = \begin{bmatrix} Z_{Rf\dot{w}} & Z_{Rf\dot{\theta}} \\ Z_{Rm\dot{w}} & Z_{Rm\dot{\theta}} \end{bmatrix} = \begin{bmatrix} \frac{1}{Z_{Rf}} & \frac{1}{Z_{Rfm}} \\ \frac{1}{Z_{Rmf}} & \frac{1}{Z_{Rm}} \end{bmatrix}^{-1} \quad (2.52)$$

These impedances are used in the theoretical analysis which characterises the response \mathbf{X} of an arbitrarily terminated beam to an applied force or moment applied at some position x_0 (Section 2.2). The impedance terms become part of the coefficient matrix $\boldsymbol{\alpha}$ in Equation

Chapter 2. Control of vibrations in a stiffened beam

(2.34). In the analysis that follows Equation (2.34), the matrix α is inverted and multiplied by a vector F or M . Both column vectors consist of seven zero elements and one non-zero force or moment term, which occurs in either the seventh or eighth position. The only columns of importance in the inverse matrix α^{-1} are the seventh and eighth columns, as all other columns will be multiplied by a zero element in the vector F or M . The practical implication of this result is that only the larger elements of the first four rows of the α matrix will affect the solution vector X . The result is that the accuracy of the solution vector X can be exactly maintained with the off-diagonal coupling elements $Z_{m\dot{w}}$ and $Z_{f\dot{\theta}}$ of the impedance matrix set to zero. This simplification is justified by examples rather than by formal proof, as inverting the complex matrix α symbolically is not practical.

Once the impedance matrix has been approximated by the equivalent matrix with just two unknowns, determining the unknown equivalent impedance of a given beam termination from experimental data is possible. Beginning with the beam shown in Figure 2.1, the unknown termination at the left hand end may be described by the equivalent impedance matrix

$$\mathbf{Z}_L = \begin{bmatrix} Z_{L1} & 0 \\ 0 & Z_{L2} \end{bmatrix} \sim \begin{bmatrix} Z_{Lf\dot{w}} & Z_{Lf\dot{\theta}} \\ Z_{Lm\dot{w}} & Z_{Lm\dot{\theta}} \end{bmatrix}. \quad (2.53)$$

Chapter 2. Control of vibrations in a stiffened beam

The right hand termination may be such that the impedance values are known, or it may be the same unknown termination used on the left hand end, in which case (following the sign conventions given in Figure 2.3) the equivalent impedance matrix \mathbf{Z}_R is given by

$$\mathbf{Z}_R = \begin{bmatrix} Z_{R1} & 0 \\ 0 & Z_{R2} \end{bmatrix} = \begin{bmatrix} -Z_{L1} & 0 \\ 0 & -Z_{L2} \end{bmatrix}. \quad (2.54)$$

The method that follows will be the same regardless of whether a known or unknown termination is used at the right hand end. Setting the coupling terms in Equations (2.7) and (2.8) to zero for our equivalent case, substituting for Z_{L1} and Z_{L2} and rearranging,

$$Z_{L1} = \frac{F}{\dot{w}} \quad (2.55)$$

and

$$Z_{L2} = \frac{M}{\dot{\theta}}. \quad (2.56)$$

For harmonic signals $\dot{w} = j\omega w$ and $\dot{\theta} = -j\omega w'$. Replacing the bending moment and shear force with derivatives of the displacement function gives

$$Z_{L1} = \frac{EI_{yy}w_1'''(x_L)}{j\omega w_1(x_L)} \quad (2.57)$$

and

$$Z_{L2} = \frac{EI_{yy}w_1''(x_L)}{j\omega_1'(x_L)}. \quad (2.58)$$

Chapter 2. Control of vibrations in a stiffened beam

All that remains is to find the displacement and derivatives required in Equations (2.57) and (2.58). The accelerations $a_1, a_2, a_3, \dots, a_n$ (relative to an arbitrary reference signal) are measured at n positions $x_1, x_2, x_3, \dots, x_n$ such that $x_L < x_i < x_0$. For $i = 1$ to n ,

$$a_{ie}(x_i) = -\omega^2 w_{ie}(x_i) = A_{1e} e^{k_b x_i} + B_{1e} e^{-k_b x_i} + C_{1e} e^{jk_b x_i} + D_{1e} e^{-jk_b x_i} \quad (2.59)$$

where the subscript e denotes experimentally obtained values. Writing in matrix form,

$$\begin{bmatrix} \frac{-a_{1e}}{\omega^2} \\ \frac{-a_{2e}}{\omega^2} \\ \frac{-a_{3e}}{\omega^2} \\ \vdots \\ \frac{-a_{ne}}{\omega^2} \end{bmatrix} = \begin{bmatrix} \beta_1 & \beta_1^{-1} & \beta_1^j & \beta_1^{-j} \\ \beta_2 & \beta_2^{-1} & \beta_2^j & \beta_2^{-j} \\ \beta_3 & \beta_3^{-1} & \beta_3^j & \beta_3^{-j} \\ \vdots & \vdots & \vdots & \vdots \\ \beta_n & \beta_n^{-1} & \beta_n^j & \beta_n^{-j} \end{bmatrix} \begin{bmatrix} A_{1e} \\ B_{1e} \\ C_{1e} \\ D_{1e} \end{bmatrix}, \quad (2.60)$$

where $\beta_i = e^{k_b x_i}$, $\beta_i^{-1} = e^{-k_b x_i}$, $\beta_i^j = e^{jk_b x_i}$ and $\beta_i^{-j} = e^{-jk_b x_i}$. Rearranging gives

$$\begin{bmatrix} A_{1e} \\ B_{1e} \\ C_{1e} \\ D_{1e} \end{bmatrix} = \begin{bmatrix} \beta_1 & \beta_1^{-1} & \beta_1^j & \beta_1^{-j} \\ \beta_2 & \beta_2^{-1} & \beta_2^j & \beta_2^{-j} \\ \beta_3 & \beta_3^{-1} & \beta_3^j & \beta_3^{-j} \\ \vdots & \vdots & \vdots & \vdots \\ \beta_n & \beta_n^{-1} & \beta_n^j & \beta_n^{-j} \end{bmatrix}^{-1} \begin{bmatrix} -\frac{a_{1e}}{\omega^2} \\ -\frac{a_{2e}}{\omega^2} \\ -\frac{a_{3e}}{\omega^2} \\ \vdots \\ -\frac{a_{ne}}{\omega^2} \end{bmatrix}, \quad (2.61)$$

where the inversion operator represents the generalised inverse or pseudo-inverse. Equation (2.61) represents a system of n equations in four unknowns. If $n = 4$, the system is determined, but the solution $(A_{1e}, B_{1e}, C_{1e}, D_{1e})$ is extremely sensitive to errors in the measured accelerations. The error is significantly reduced if an overdetermined system is used ($n > 4$), as will be shown.

Table 2.3

Beam Parameters for Impedance Accuracy Calculations

Parameter	Value
Beam length L_x	10.0 m
Beam width L_y	0.05 m
Beam height L_z	0.025 m
Young's modulus E	71.1 GPa
Excitation force location x_0	0.0 m
Excitation frequency f	1000 Hz
Wavelength λ_b	0.4824 m

Let w_e be the displacement calculated from the constants A_{1e} , B_{1e} , C_{1e} and D_{1e} . For the beam described by the parameters of Table 2.3 with end conditions modelled as infinite, the error induced in the displacement w_e , given an initial error in the real and imaginary parts of the accelerations $(a_i, i = 1, n)$ of 10%, is plotted as a function of the number of acceleration measurements n in Figure 2.23. For the two frequencies shown, $n \geq 10$ provides a reasonable accuracy. The higher the frequency, the greater the number of acceleration measurements that will be required. Measurements do not need to be made simultaneously, so a couple of accelerometers can be used and placed at each of the measurement positions in turn.

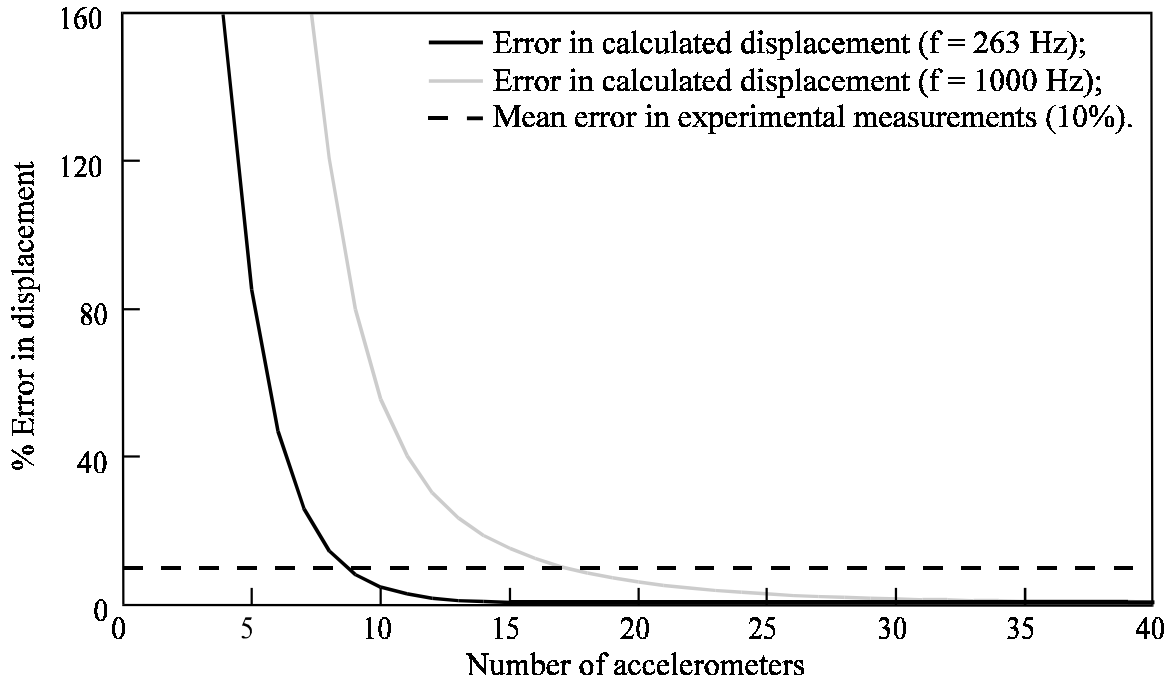


Figure 2.23 Error in displacement calculated using "measured" impedances with a mean experimental error of 10%.

Once calculated, A_{1e} , B_{1e} , C_{1e} and D_{1e} are substituted into Equation (2.3) and differentiation is carried out to find $w_{1e}(x_L)$, $w'_{1e}(x_L)$, $w''_{1e}(x_L)$ and $w'''_{1e}(x_L)$. Equations (2.57) and (2.58) can then be used to find the equivalent impedances Z_{L1} and Z_{L2} .

It should be noted that use of the "equivalent" impedance matrix obtained by eliminating the off-diagonal elements from the impedance matrix is only valid for analyses similar to that followed in this chapter. It is not claimed that the resulting impedance matrix closely approximates the real impedance values of the termination in general circumstances. However, the numerical answers for all derivatives of displacement (and hence acceleration etc.), calculated at any point along the beam, are correct to the accuracy of the calculating

Chapter 2. Control of vibrations in a stiffened beam

program (eight figures in the work done for this chapter) when compared to the corresponding derivatives obtained by using the "exact" impedance matrix. Furthermore, it is found that the most significant elements of the equivalent impedance matrix so approximated are at least similar if not precisely the same as the corresponding elements of the exact impedance matrix.

The accuracy of this method has been tested with a variety of cases. The "exact" impedance matrices and the corresponding approximations calculated using the method described are given in Table 2.4. All of these examples utilise a right hand impedance corresponding to an ideally infinite beam, and approximations are made for the various test cases at the left hand end of the beam. The parameters characterising the beam are given in Table 2.3. For all the examples, all derivatives of displacement calculated using the "exact" and equivalent impedance matrices are either identical, or are insignificantly small.

It would be expected that the simplification might fail when the original matrix had large elements on the off-diagonal, but this is not the case, as shown by the first two examples in Table 2.4. The third example shows an approximation for an impedance matrix with four complex elements. Examples 4, 5 and 6 show the exact and equivalent matrices for the ideal infinite, free and fixed beam impedances respectively.

Table 2.4

Impedance Matrices and Corresponding Equivalent Matrices

E.g. No.	"Exact" Matrix Z_L	Corresponding Equivalent Matrix (with zero off-diagonal elements)
1	$\begin{bmatrix} 0 & -10^{100} - 10^{100}j \\ 10^{100} + 10^{100}j & 0 \end{bmatrix}$	$\begin{bmatrix} -1.61 \times 10^{19} - 9.30 \times 10^{18}j & 0 \\ 0 & 2.44 \times 10^{15} - 5.00 \times 10^{16}j \end{bmatrix}$
2	$\begin{bmatrix} 0 & -10^{100} \\ 10^{100} & 0 \end{bmatrix}$	$\begin{bmatrix} -2.07 \times 10^{19} - 1.27 \times 10^{18}j & 0 \\ 0 & 1.01 \times 10^{17} - 4.28 \times 10^{16}j \end{bmatrix}$
3	$\begin{bmatrix} 5 + 6j & 7 + 8j \\ 1 + 2j & 3 + 4j \end{bmatrix}$	$\begin{bmatrix} 222.4 + 10.89j & 0 \\ 0 & 4.963 + 6.101j \end{bmatrix}$
4	$\begin{bmatrix} -1628 - 1628j & -125.0 \\ 125.0 & 9.596 - 9.596j \end{bmatrix}$	$\begin{bmatrix} -1628.0 & 0 \\ 0 & 9.596 \end{bmatrix}$
5	$\begin{bmatrix} 0 & 0 \\ 0 & 0 \end{bmatrix}$	$\begin{bmatrix} 5.6 \times 10^{-14} - 1.3 \times 10^{-13}j & 0 \\ 0 & -1.5 \times 10^{-15} - 2.8 \times 10^{-16}j \end{bmatrix}$
6	$\begin{bmatrix} 10^{100} & 0 \\ 0 & 10^{100} \end{bmatrix}$	$\begin{bmatrix} -1.38 \times 10^{19} - 8.48 \times 10^{17}j & 0 \\ 0 & 5.00 \times 10^{15} - 8.13 \times 10^{16}j \end{bmatrix}$

Four different beam terminations were used in the experimental verification of the beam model. For the simple support, the wire support and the anechoic termination, classical impedances are given in Table 2.5 (with the wire support modelled as a free end and the anechoic termination modelled as an infinite end). The fourth termination used was a simply supported termination mounted on vibration isolators, for which a theoretical impedance is

not easily calculated. Using the method outlined, new impedance matrices were calculated from the experimentally measured uncontrolled acceleration distribution for each end condition. These matrices are also listed in Table 2.5, and differ considerably from the classical theoretical impedances for the three modelled terminations.

Table 2.5
Classical and Calculated Impedance Matrices

Termination	Classical Impedance Matrix Z_L	Calculated Impedance Matrix Z_L
Wire Supported ("Free")	$\begin{bmatrix} 0 & 0 \\ 0 & 0 \end{bmatrix}$	$\begin{bmatrix} -109 + 124j & 0 \\ 0 & 3.25 + 6.30j \end{bmatrix}$
Simply Supported	$\begin{bmatrix} \infty & 0 \\ 0 & 0 \end{bmatrix}$	$\begin{bmatrix} 3961 + 522j & 0 \\ 0 & 8.32 + 8.21j \end{bmatrix}$
Anechoic ("Infinite")	$\begin{bmatrix} -834 - 834j & 125.0 \\ -125.0 & 18.7 - 18.7j \end{bmatrix}$	$\begin{bmatrix} 1440 - 1061j & 0 \\ 0 & 5.46 + 7.36j \end{bmatrix}$
Vibration Isolated	None	$\begin{bmatrix} -539 - 834j & 0 \\ 0 & 6.75 + 7.71j \end{bmatrix}$

2.4.2 Relating control signal and control force

To relate experimental results to theoretical calculations, it is necessary to determine the input voltage required to drive the piezoceramic stack actuator to produce a unit output force F_s . To begin, the stiffness of the stiffener is approximated by modelling the stiffener (Figure 2.24) as two beams (Figure 2.25).

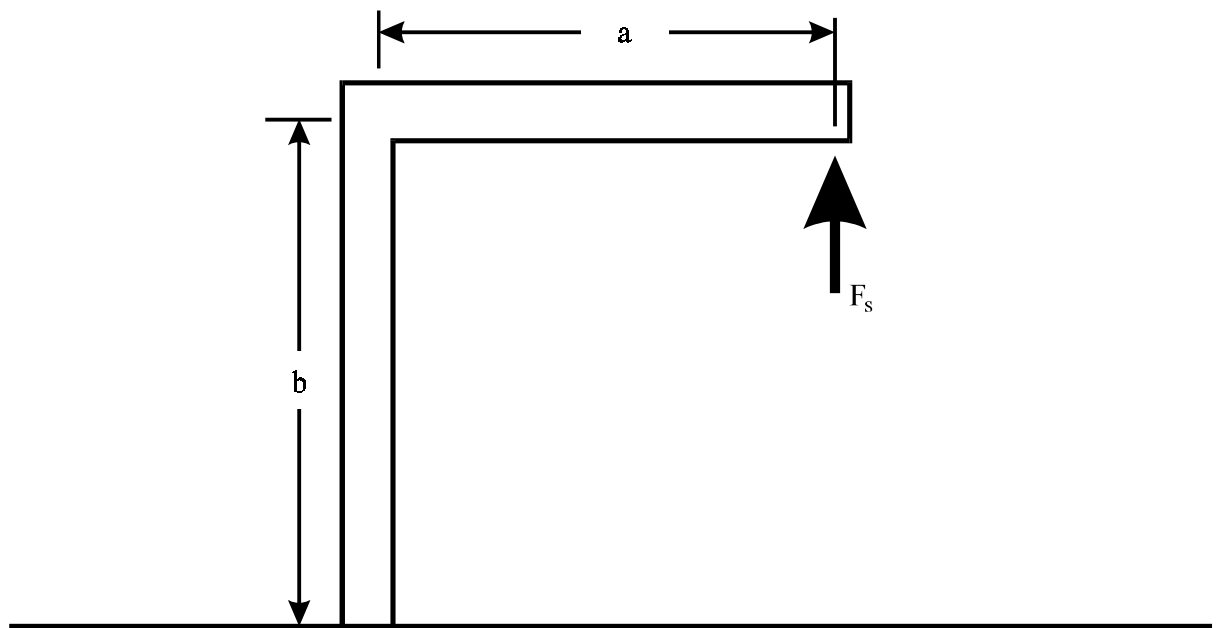


Figure 2.24 Stiffener showing dimensions.

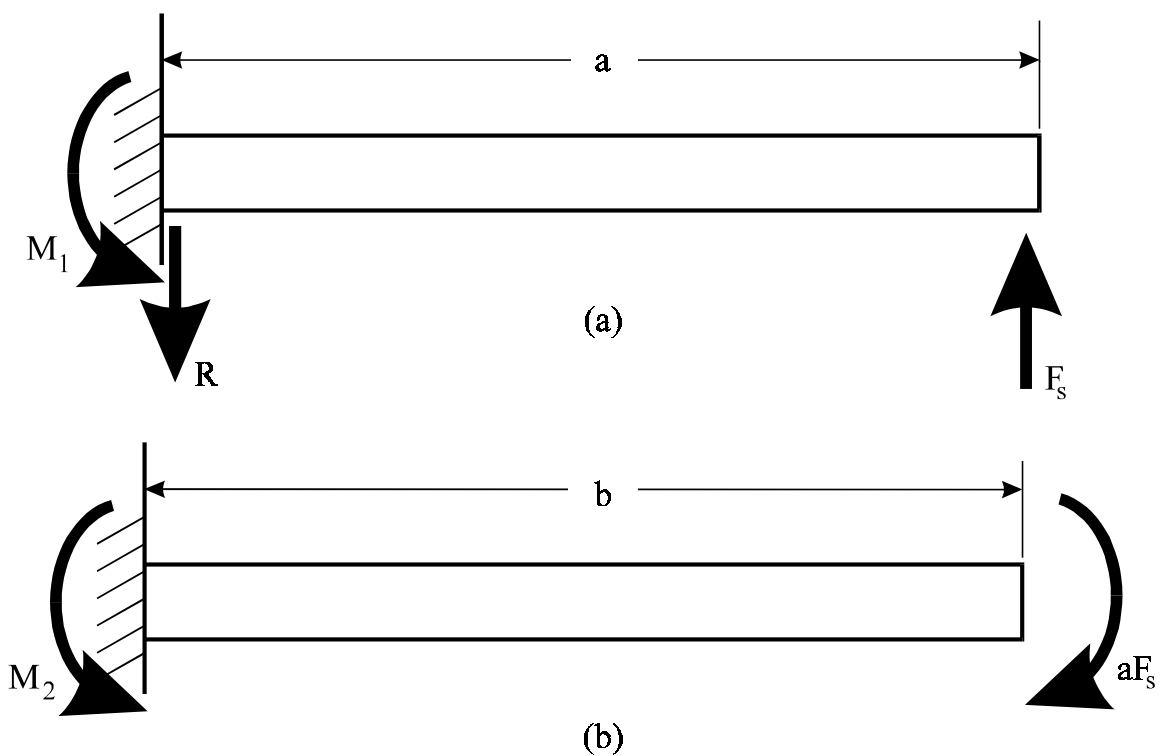


Figure 2.25 Stiffener flanges modelled as beams; (a) horizontal stiffener flange, and (b) vertical stiffener flange.

Chapter 2. Control of vibrations in a stiffened beam

The first beam is characterised by a length x_a , with a load F_s at one end and a rigid support at the other. The support provides a vertical reaction $R = F_s$ and moment reaction $M_1 = aF_s$ as shown. Taking the origin of coordinates to be the support end, the equation for the bending moment in this beam is

$$\begin{aligned} M &= M_1 - Rx = F_s(a - x) \\ \Rightarrow EI_{yy}w_a''(0) &= F_s(a - x) , \end{aligned} \quad (2.62)$$

where $w_a(x)$ is deflection at position x , E is Young's modulus and I_{yy} is the second moment of area about the y -axis. Integrating twice and using the boundary conditions $w_a(0) = 0$ and $w_a'(x) = 0$,

$$\begin{aligned} w_a(x) &= \frac{F_s}{EI_{yy}} \left(\frac{ax^2}{2} - \frac{x^3}{6} \right) , \\ \therefore w_a(a) &= \frac{F_s a^3}{3EI_{yy}} . \end{aligned} \quad (2.63)$$

Denoting the deflection of the beam of length b in Figure 2.25(b) by $w_b(x)$, and using the reaction $M = aF_s$ as shown, the bending moment equation is

$$M_2 = EI_{yy}w_b''(x) = bF_s . \quad (2.64)$$

Integrating and using the boundary condition $w_b'(0) = 0$,

$$EI_{yy}w_b'(b) = F_s b^2 . \quad (2.65)$$

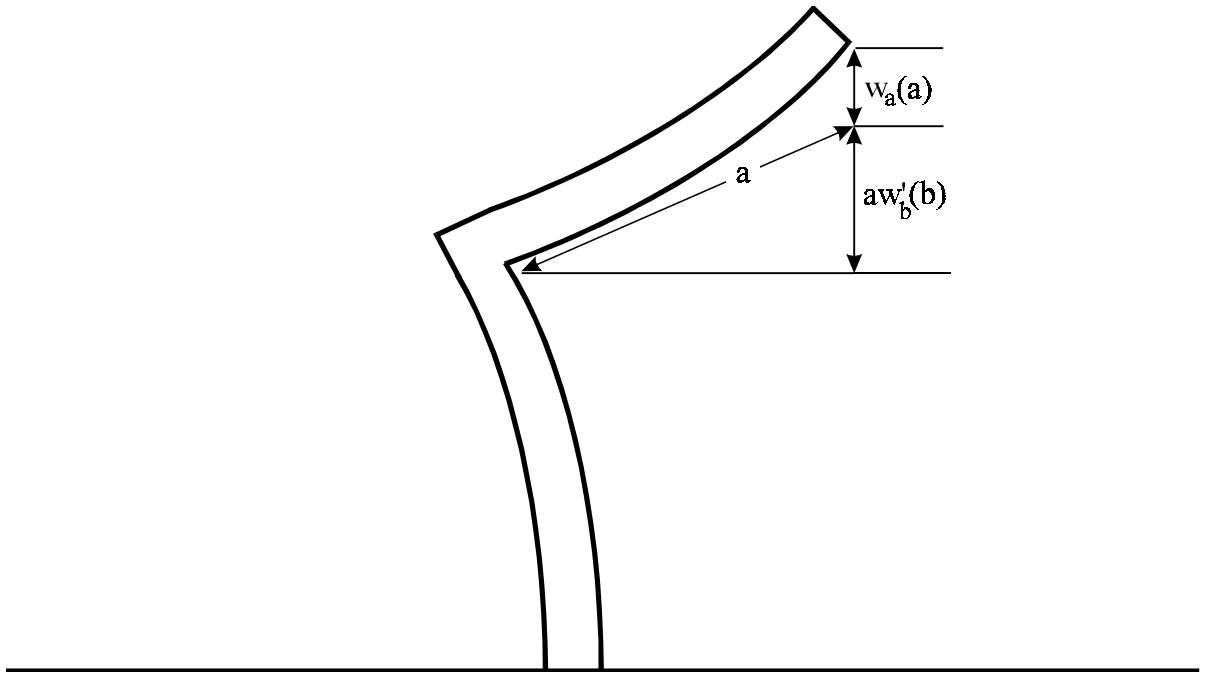


Figure 2.26 Displaced angle stiffener.

The vertical total deflection of the stiffener at the position of the actuator force F_s is approximately $w = w_a(a) + aw'_b(b)$ (Figure 2.26). Thus

$$w = \frac{F_s}{EI_{yy}} \left(\frac{a^3}{3} + ab^2 \right) . \quad (2.66)$$

Stiffness is defined as force per unit displacement, so the equivalent stiffness of the stiffener is

$$k_s = \frac{F_s}{w} = \frac{EI_{yy}}{(a^3/3 + ab^2)} . \quad (2.67)$$

Now the piezoceramic stack voltage required to produce a resultant force F_s is calculated.

The maximum force F_{max} generated by the actuator with an input voltage V_0 is

$$F_{\max} = k_a \Delta L_0 \left(1 - \frac{k_a}{k_a + k_s}\right) = \Delta L_0 \left(\frac{k_a k_s}{k_a + k_s}\right), \quad (2.68)$$

where ΔL_0 is the nominal expansion of the actuator, k_a is the spring constant of the actuator and k_s is the spring constant of the stiffener. The applied potential difference V to achieve a resultant force F_s is given by

$$\frac{V}{V_0} = \frac{F_s}{F_{\max}}, \quad (2.69)$$

or

$$V = F_s \times \left[\frac{V_0 (k_a + k_s)}{\Delta L_0 k_a k_s} \right]. \quad (2.70)$$

Equation (2.67) can be used to find k_s , which can then be substituted into Equation (2.70) along with data for a stack actuator to find the required potential difference input for a unit force output; alternatively, Equation (2.70) can be rearranged to find the force resulting from a given input potential.

2.4.3 Test procedure

A steel stiffener was bolted tightly to an aluminium beam described by the dimensions given in Table 2.6. The piezoceramic actuator with the characteristics listed in Table 2.7 was placed between the stiffener flange and the beam.

Table 2.6
Beam Parameters for Experimental Results

Parameter	Value
Beam length L_x	3.9 m
Beam width L_y	0.05 m
Beam height L_z	0.025 m
Young's modulus E	71.1 GPa
Primary force location x_p	0.0 m
Control location x_1	0.5 m (= $0.53\lambda_b$)
Error sensor location x_e	1.0 m (= $1.06\lambda_b$)
Excitation frequency f	263 Hz
Wavelength λ_b	0.94 m

Table 2.7
Angle and Actuator Parameters for Experimental Results

Parameter	Value
Stiffener flange length a	0.05 m
Angle height b	0.05 m
Angle width d	0.05 m
Angle thickness t	0.01 m
Young's modulus E	210 GPa
Physik Instrumente Translator No.	P244.20
Actuator spring constant k_T	38 N/ μ m
Nominal expansion of actuator ΔL_0	20 μ m
Nominal voltage V_0	-1000 V

The actuator was attached only at one end to ensure that no external tensile force was applied to it, as the type of actuator used is weak in tension. The primary source, control source and error sensor locations and the excitation frequency are also given in Table 2.6. The beam was mounted with the larger width dimension in the vertical plane, and excited in the horizontal plane.

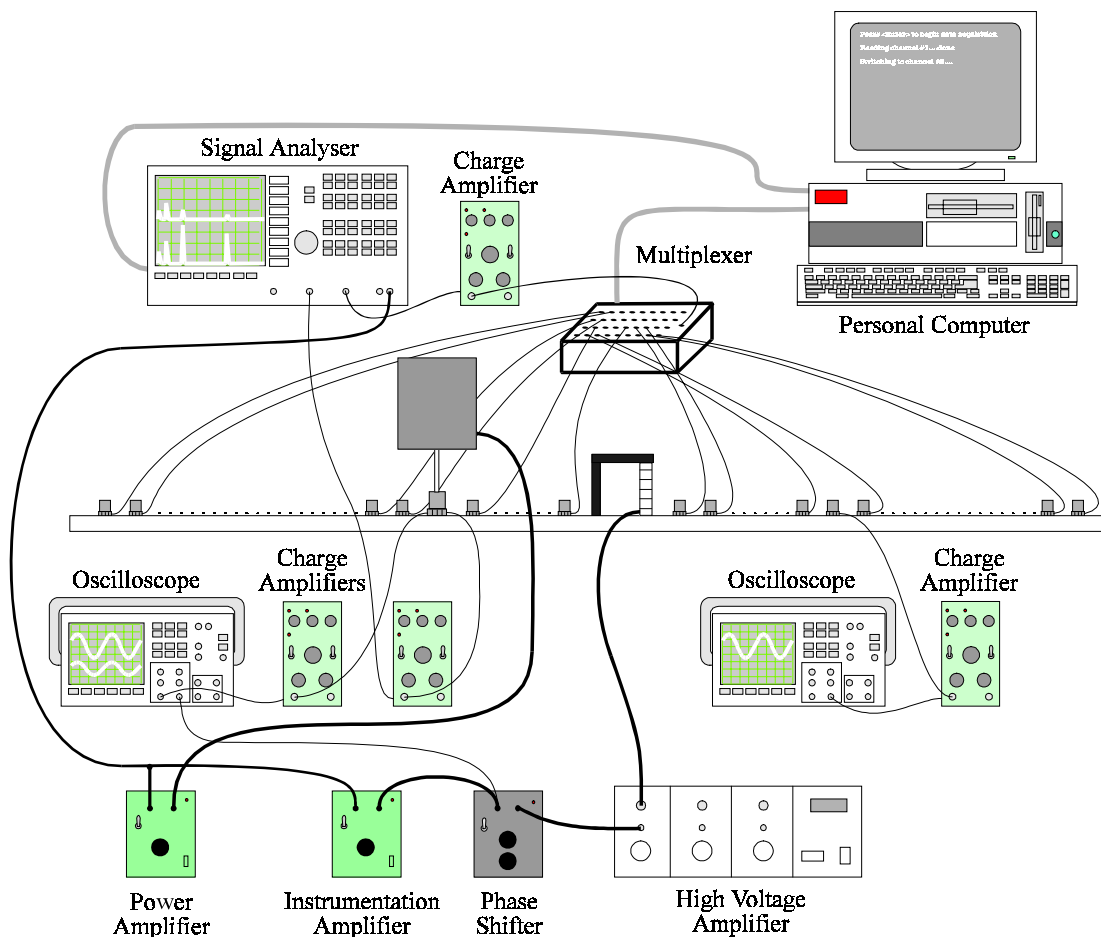


Figure 2.27 Experimental arrangement for the active control of vibration in a beam.

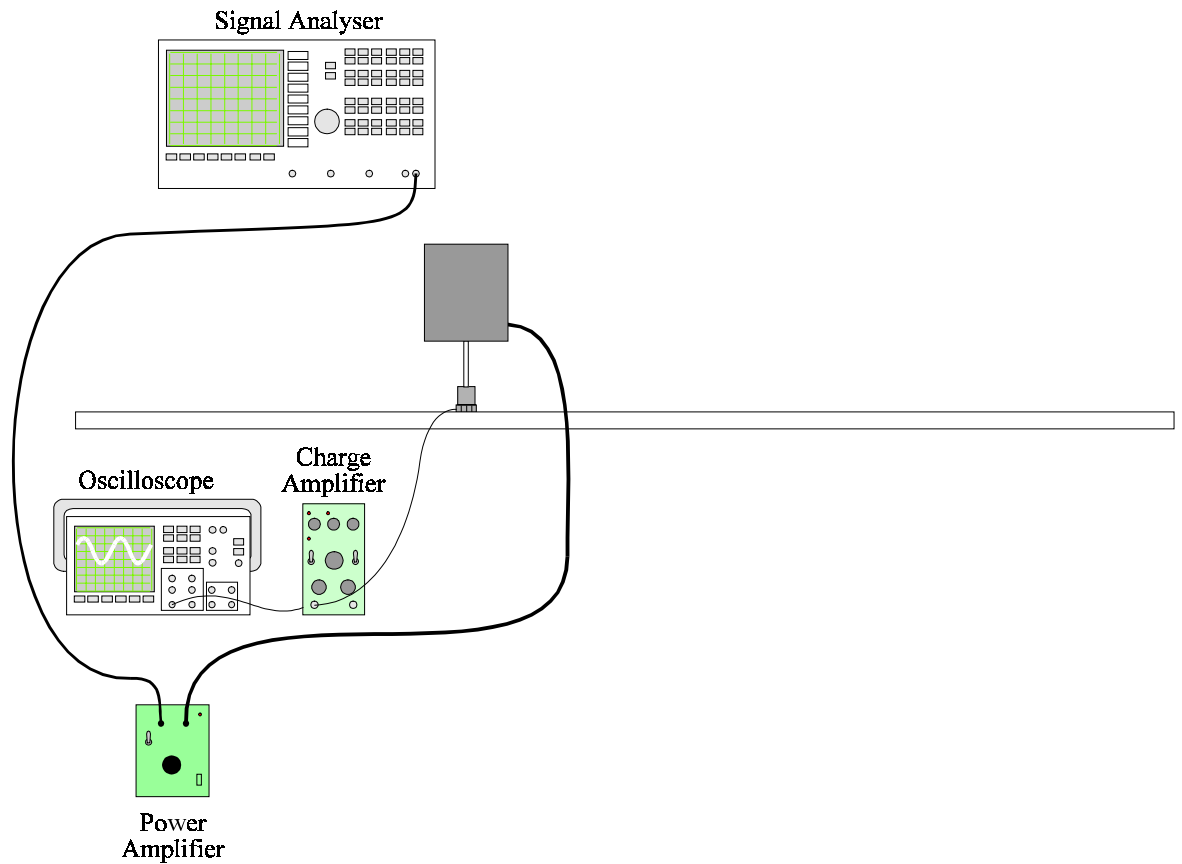


Figure 2.28 Primary system.

The complete experimental arrangement is given in Figure 2.27. The primary signal was produced by a signal analyser and amplified to drive the electrodynamic shaker (Figure 2.28).

The shaker acted on the beam through a force transducer, and the magnitude of the primary force was recorded using an oscilloscope.

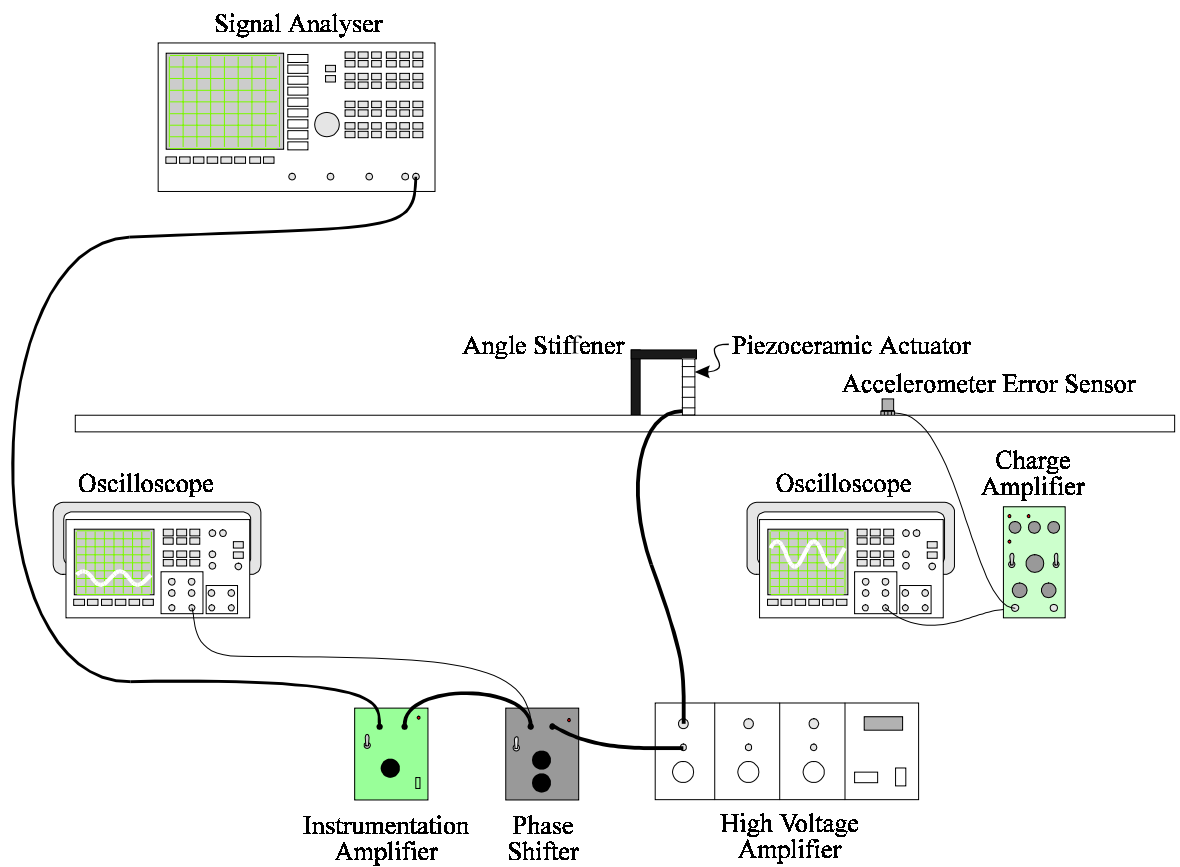


Figure 2.29 Control system.

The error signal from the accelerometer (Figure 2.29) was passed to another oscilloscope. The amplitude and phase of the primary signal were adjusted using an instrumentation amplifier and a phase shifter to produce the control signal, which drove the piezoceramic actuator. The control signal was adjusted to optimally minimise the acceleration measured by the error sensor accelerometer. The control signal was also recorded using an oscilloscope.

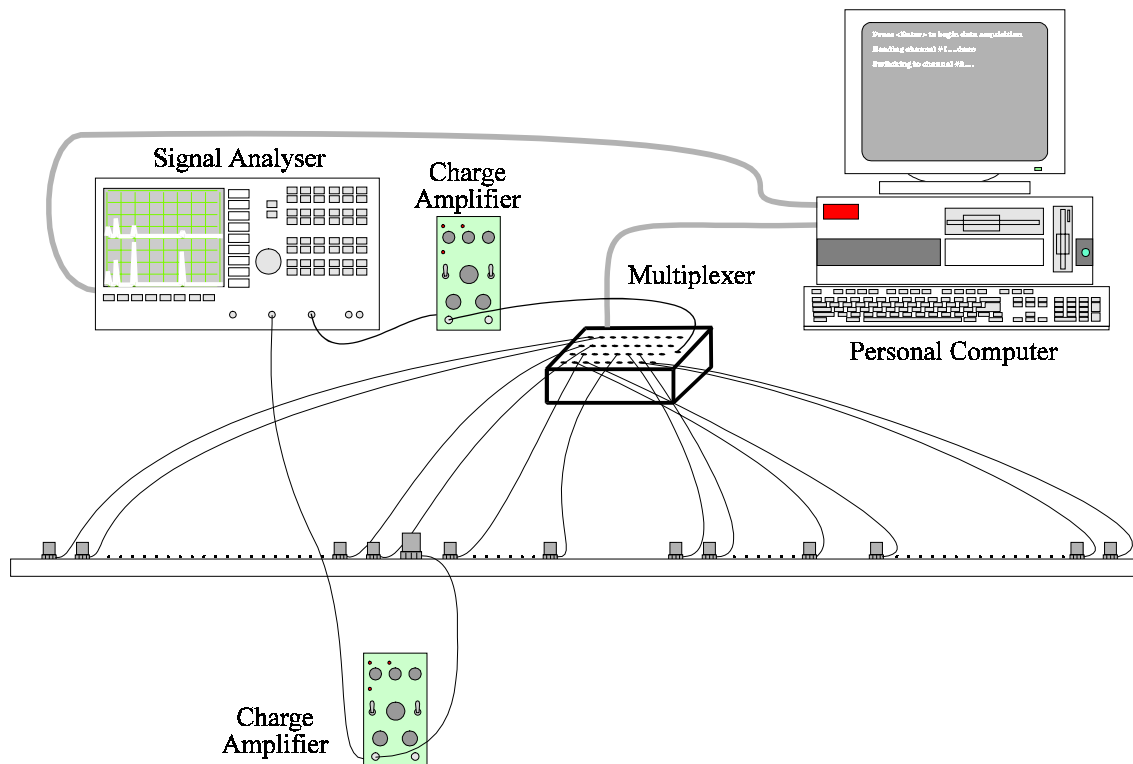


Figure 2.30 Acceleration measurement.

The acceleration was measured at 5 cm intervals along the beam (Figure 2.30). The accelerometer signals were read in turn through a 40 channel multiplexer and passed to a Hewlett-Packard type 35665A signal analyser. The frequency response function was used to analyse the data. The magnitude and phase of the acceleration were recorded on a personal computer, which was also used to switch the recorded channel on the multiplexer. The acceleration output of the force transducer at the primary location was used as the reference signal for the frequency response analysis. Accelerometer readings were taken initially once the error sensor signal had been optimally reduced, and again with the control amplifier switched off (the uncontrolled case).

Chapter 2. Control of vibrations in a stiffened beam

Figures 2.31 - 2.33 show photographs of the experimental equipment. In Figure 2.31, the beam is located in front of the signal generating and recording equipment. The electromagnetic shaker primary source, angle stiffener and accelerometers can be seen connected to the beam. The piezoceramic stack actuator and angle stiffener are shown close-up in Figure 2.32, and one end of the beam supported by the wire termination is shown in Figure 2.33.

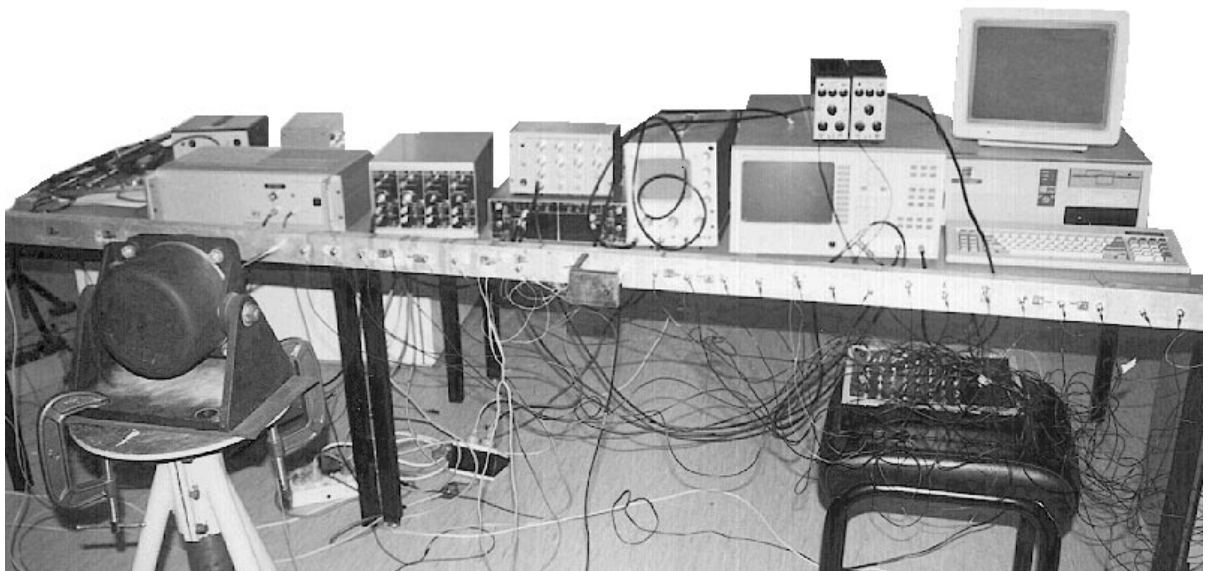


Figure 2.31 Experimental equipment for the active control of beam vibration.

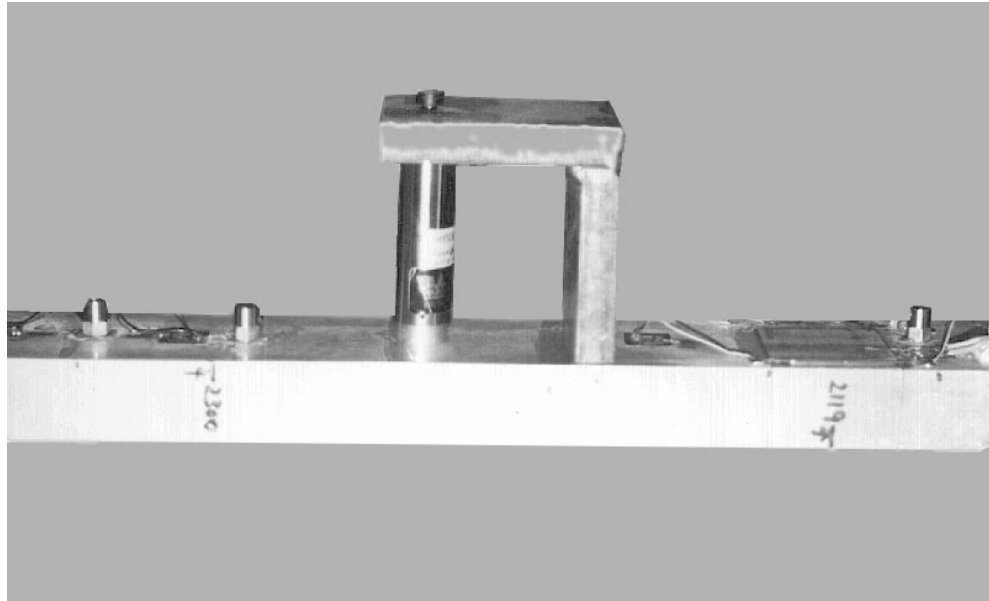


Figure 2.32 Piezoceramic stack actuator mounted between the beam and the flange of the angle stiffener.

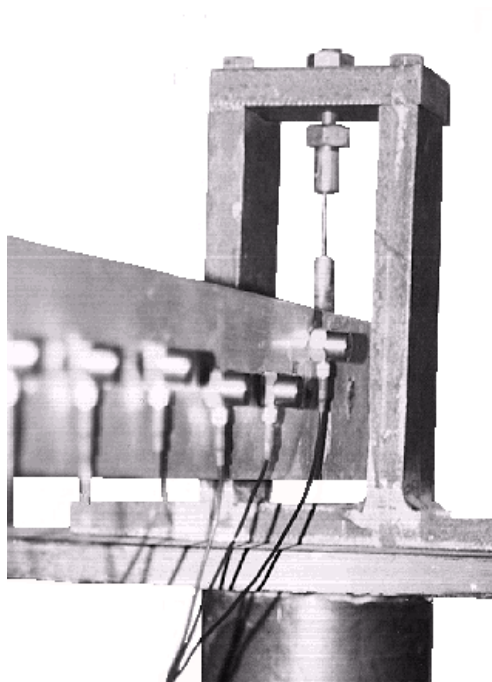


Figure 2.33 Beam termination with wire support.

2.5 EXPERIMENTAL RESULTS

To verify the theoretical model, the experiment described in Section 2.4 was repeated for four different terminations. For the simple support, the wire support and the anechoic termination, classical impedances are given in Table 2.5 (with the wire support modelled as a free end and the anechoic termination modelled as an infinite end). The fourth termination used was a simply supported termination mounted on vibration isolators, for which there is no classical theoretical impedance. Using the method described in Section 2.4.1, new impedance matrices were calculated from the experimental acceleration distribution for each end condition. These matrices are also listed in Table 2.5, and differ considerably from the classical theoretical impedances for the three modelled terminations.

Figure 2.34 shows the controlled and uncontrolled acceleration distributions corresponding to the classical impedance, as well as the corresponding curves for the calculated impedances with the experimental results overlaid, for the anechoic termination. Figures 2.35 and 2.36 show similar results for the wire supported and simply supported beams. These figures show that agreement is far closer between the experimental results and the theoretical results obtained with the calculated impedances than between the experiment and the theoretical results obtained using the classical impedance values. The classical impedance matrices do not model accurately the real supports used in this experiment.

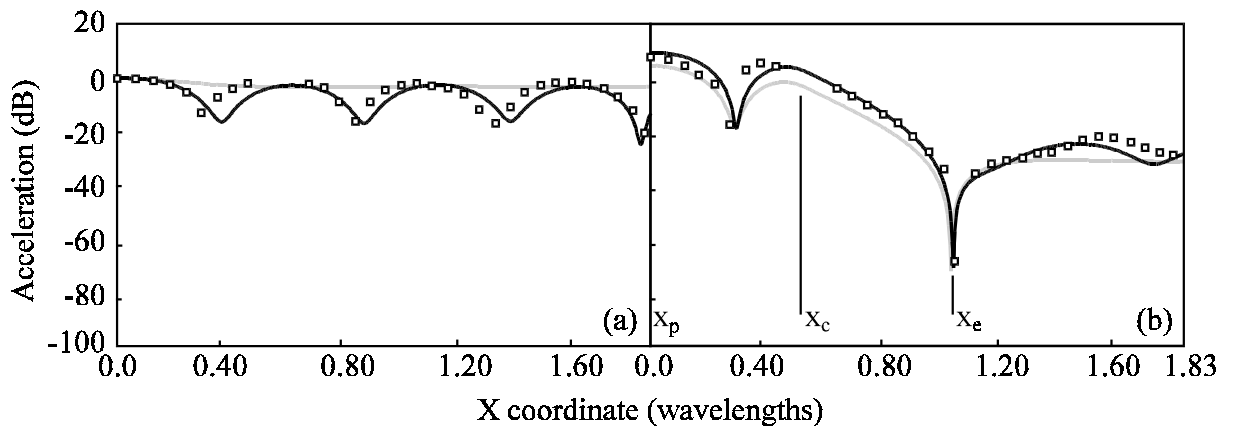


Figure 2.34 Acceleration distributions for the anechoically terminated beam.

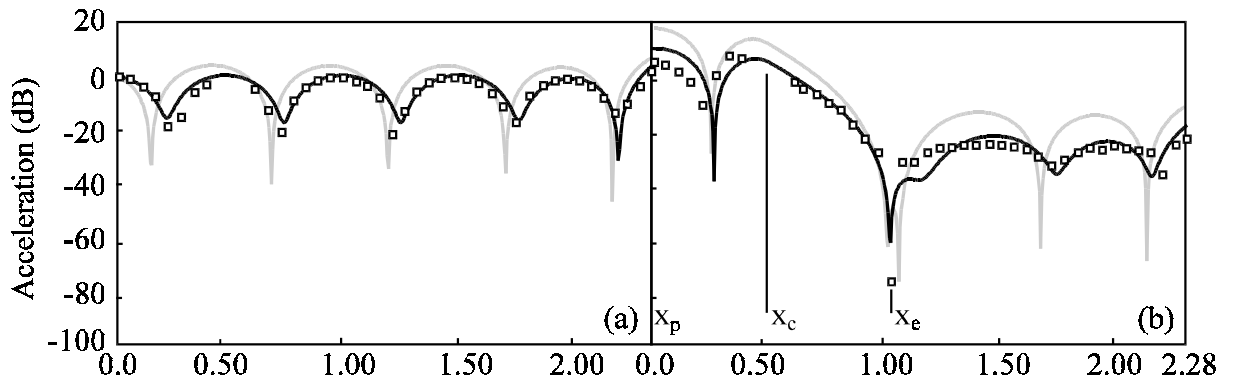


Figure 2.35 Acceleration distributions for the wire supported beam.

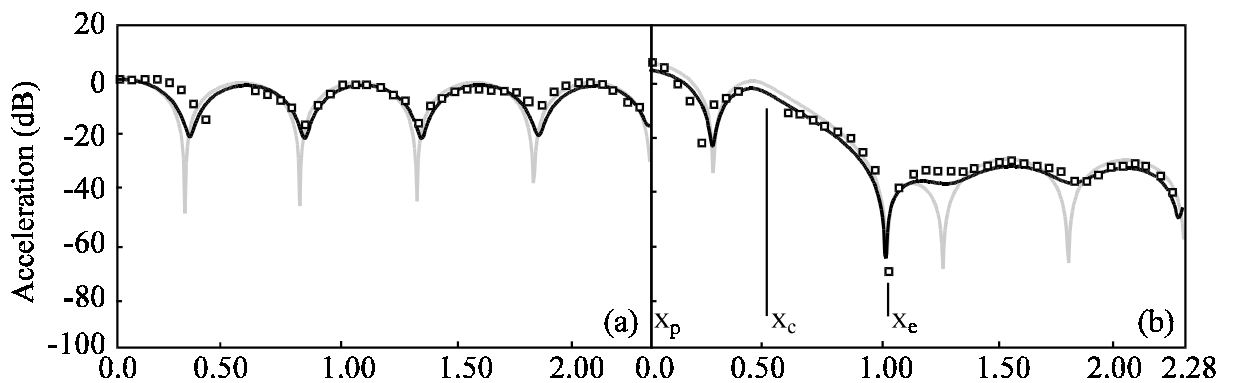


Figure 2.36 Acceleration distributions for the simply supported beam.

(a) Uncontrolled case; (b) Controlled case. — Theoretical results, classical impedance;
 — Theoretical results, calculated impedance; ◻ Experimental data.

x_p = primary source location; x_c = control source location; x_e = error sensor location.

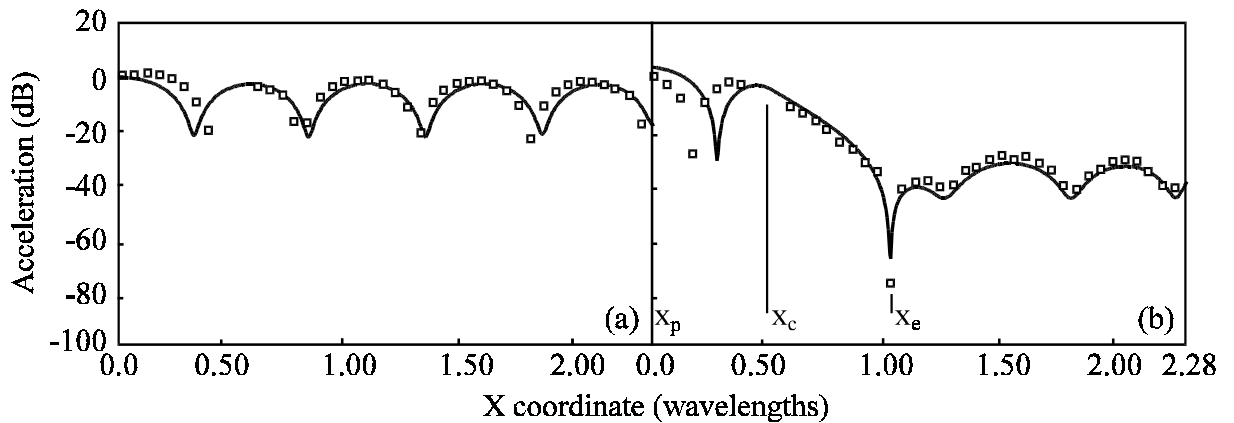


Figure 2.37 Acceleration distributions for the vibration isolated beam.

(a) Uncontrolled case; (b) Controlled case. — Theoretical results; \square Experimental data.
 x_p = primary source location; x_c = control source location; x_e = error sensor location.

Figure 2.37 shows the calculated impedance curves with experimental data for the vibration isolated beam, but no classical impedance curves are given for this case as there is no known classical impedance for this arrangement. The theoretical curves corresponding to calculated impedances shown in the figures for the uncontrolled and controlled cases and for all end conditions show very good agreement with the experimental data.

The main area of difference between the calculated impedance theoretical acceleration curves and the experimental data is the location of the first minima to the right of the primary force. In the uncontrolled cases, the first minima in the theoretical curve occurs slightly to the left of the experimental minima (except in the anechoic termination case). In the controlled cases, the first minima in the theoretical curves are slightly to the right of the experimental results.

Chapter 2. Control of vibrations in a stiffened beam

All of these minima occur within half a wavelength of the primary source (and in the controlled cases, also of the control source), and this may indicate that the theory is limited in approximating the effect of the near field.

Table 2.8 compares the theoretical and experimental control force relative to the primary force for each end condition. The primary force was measured using a force transducer placed between the primary shaker and the beam. The control force magnitude was estimated by the procedure outlined above, using Equations (2.60) and (2.63). Again, agreement is good, although it should be said that the control force calculation is dependent on a number of assumptions and should only be used as an order of magnitude calculation.

Table 2.8

Comparison Between Experimental and Theoretical Control Forces

End Condition	Theoretical Amplitude*	Experimental Amplitude*	Theoretical Phase*	Experimental Phase*
Wire Support	5.20	4.93	0 or 180	0 or 180
Simple Support	1.69	1.72	0 or 180	0 or 180
Anechoic	2.43	2.53	0 or 180	0 or 180
Vibration Isolated	2.32	2.38	0 or 180	0 or 180

*Control force amplitude and phase are expressed relative to the primary force.

2.6 SUMMARY

A theoretical model has been developed to describe the vibration response of an arbitrarily terminated beam to a range of excitation types, and in particular to describe the vibration response of beams to a point force primary excitation source and angle stiffener and piezoceramic stack control source. The numerical results indicate that flexural vibrations in beams can be actively controlled using the piezoceramic stack actuator and angle stiffener control source. Numerical results also indicate:

- (1) The magnitude of the control source required for optimal control generally decreases with increasing stiffener flange length (see Figure 2.6 for definition of stiffener flange length) and increasing frequency.
- (2) The control source amplitude required for optimal control is less when the beam is excited at a resonance frequency.
- (3) When there is reflection from the beam terminations, the optimum control force is either in phase or 180° out of phase with the primary source. When there is no reflection from beam terminations (the infinite beam case), the control source phase cycles through 180° as the excitation frequency is increased.

Chapter 2. Control of vibrations in a stiffened beam

- (4) For all but the infinite beam, maxima occur in the control source amplitude required for optimal control when the separation between control and primary sources is given by $x = (c + n\lambda_p/2)$ where n is an integer and c is a constant dependent on frequency and termination type. These maxima occur when the control source is located at a node in the standing wave generated by reflection from the beam terminations. Minima in the mean attenuation of acceleration level downstream of the error sensor occur when the control source is located at a node in the standing wave.
- (5) Increasing the separation between the primary and control source does not improve attenuation.
- (6) The amount of attenuation achieved downstream of the error sensor increases with increasing separation between the error sensor and the control source.
- (7) When the error sensor is located at a node in the standing wave that exists in finite beams, the attenuation achieved is less than that achieved with the error sensor located away from a node. Locating the error sensor at a node does not affect the control source required for optimal control.
- (8) It is possible to achieve reductions in acceleration level upstream of the primary

Chapter 2. Control of vibrations in a stiffened beam

source as well as the desired reduction downstream of the error sensor. The maximum mean attenuation in acceleration level upstream of the primary source is theoretically achieved with the separation between primary and effective control source locations given by $x = (0.25 + n\lambda_b/2)$ for $n = 1,2,3\dots$

- (9) For error sensor locations outside the control source near field, the mean attenuation of acceleration level upstream of the primary source does not depend on error sensor location.

- (10) A second control source can be used to overcome the difficulty in controlling vibration when the first control source is located at a node in a standing wave. The magnitude of the first control source can be arbitrarily limited and the second control source used when the limit is reached. The maxima in control source amplitude and the minima in attenuation that occur when the first control source is located at a standing wave node are eliminated in this way.

- (11) There is no practical method of using a second error sensor to eliminate the minima in attenuation that occur when the first error sensor is located at a standing wave node.

The theoretical model outlined was verified experimentally for the four end conditions tested

Chapter 2. Control of vibrations in a stiffened beam

in this paper. The impedance corresponding to each termination was first calculated from experimental data. Comparison between experimental results and theoretical predictions showed that:

- (1) The accuracy of the theoretical model when compared to the experimental results is very high, both in predicting the control source amplitude and phase required relative to the primary source, and in determining the acceleration distribution occurring along the beam.
- (2) The impedances calculated from experimental measurements give more accurate results than the "classical" impedances corresponding to each termination.
- (3) The theoretical model accurately predicts the amount of attenuation that can be achieved experimentally.